UNIVERSITY OF COPENHAGEN
FACULTY OF SCIENCE

Master Thesis

Clara Ferreira Cores

Shallowness and susceptibility:

Tidal disruptions in DM halos simulations

Supervisors: Axel Widmark & Steen Hansen

Handed in: 20th of May 2022

Abstract

Dark Matter (DM) is one of the greatest building blocks of our Universe, amounting to 26% of its content, yet still remaining pretty much a mystery. DM simulations of structure formation predict dwarf galaxies to be located within central dense cuspy DM halos. However, their observed velocity profiles point towards constant density cores. This is one of the main issues within the current cosmological model, known as the cusp-core problem. Dwarf galaxies are great laboratories to probe into the dynamics of DM, given its particle nature, since they are of the most DM dominated structures in our Universe, avoiding 'contamination' from standard astrophysical sources. Furthermore, the increasingly accurate observational data from these satellite galaxies, has uncovered peculiar phase-space correlations, and signs of tidal disturbance in their distribution. Therefore, the great pull exerted on them by the gravitational forces of their host galaxy would influence their equilibrium state, regardless of their density profile. Still, many of them keep showing a spherical morphology. The goal of this thesis was to study how these tidal disruptions would affect each of the profiles proposed, looking for short-term non-equilibrium kinematic signatures. To this end, I built a collisionless N-body simulation, in which I used truncated Navarro-Frenk-White density profiles to recreate the cusp and core DM halos. Each of the models was set in orbit around a simulated spherically symmetric potential of the Milky Way, finding a clear difference between their dynamical response to the tidal disruption. This distinction gives us a test to compare our kinematic data against, which could become a powerful tool in our search to constrain the nature of DM that will satisfy observations.

Acknowledgements

Thank you to my supervisors: to Axel Widmark, for the continuous advice, and the learning experience this project has been; and Steen Hansen for the help with the writing of this thesis. Thank you to my family and loved ones, their limitless support and faith in me has been fundamental to the completion of this project. Finally, special mention to Rune, whose existence and living room helped reaching the finish line.

Contents

1 Introduction

The cusp-core problem has been an issue in the standard cosmological model for over two decades, since N-body simulations were able to resolve non-linear structure formation in our expanding Universe (Frenk & White, 2012). Dark matter (DM) halos are basic non-linear units of cosmic structure, with galaxies condensing at their cores. The presence of such halos was inferred from the high rotational velocities of spiral galaxies, which instead of dropping with the radius as expected from Keplerian motion, $v_c \propto r^{1/2}$, they remained constant. This could be accounted for if mass increased with radius from the central region, however such matter didn't radiate as standard baryonic matter does. This non-visible matter would account for as much as 90% of the galaxy mass, forming a spherical halo which surrounds galaxies (Arun et al., 2017). Therefore, understanding the basic properties of halos, their formation and internal structure, is key to the exploration of galaxy evolution, as well as to test our cosmological paradigms.

Resolving the formation and structure of DM halos, a collisionless collapse of a spherical perturbation in an expanding universe, was a great challenge. In order to incorporate all the non-linear gravitational effects, analytical investigations shifted towards N-body simulations in the 1980s (Del Popolo, 2009). The numerical approach of these computer simulations provided a quantitative exploration of non-linear structure against which observational data could be compared. Thus, N-body simulations advanced the field of cosmology greatly, allowing to visualise the effects of the different initial conditions each cosmological theory proposed. In fact, that was how a top-bottom scenario of large scale structure formation, meaning Hot Dark Matter (HDM), was discarded (Frenk & White, 2012). Instead, the current understanding is that halos form hierarchically through mostly minor merger of objects. In this "inside-out" picture, the halo formation would be initiated by the collapse of a strongly bound core with material being gradually added on less bound orbits. When simulating the gravitational collapse of halos in a expanding Universe, a general form of halos' spherically-averaged density profiles was uncovered. This universal form is followed regardless of the mass of the halo or cosmology model; it was coined as the Navarro-Frenk-White (NFW) profile (Navarro et al., 1996b). Although the spherically-averaged density profiles of N-body DM halos are similar, independently of the model, their profiles are significantly different from the single power laws predicted by the theoretical studies. The numerical simulations produce a cuspy density profile, yet the observed rotation curves from dwarf galaxies indicates that the shape at small scales is shallower, leaning towards a constant density core (Del Popolo, 2009). There is

not a consensus on the shape of the density profile, showing the difficulty of simulating the innermost structure of halos in a reliable way even nowadays. Further complications emerge if we are to consider the baryonic component of a galaxy and the possible interactions (Del Popolo & Le Delliou, 2021). However, such baryonic effects should be minimal in very faint DM dominated galaxies, as for instance in dwarf galaxies, because the total fraction of mass in baryonic form is too small to be able to affect gravitationally the DM component (Errani et al., 2022).

Dwarf spheroidal galaxies (dSph) are of the oldest structures in our Universe, and are believed to be the most dark matter (DM) dominated stellar systems known. They are elemental in the standard hierarchical galaxy formation models, as these satellites are believed to be disrupted tidally into streams that merge within their host galaxy, making them key pieces to our understanding of normal sized galaxies as well (Alarcón Jara et al., 2018). Given their old age, dSphs rarely have star formation or gas left, and are composed of just a billion of stars. Therefore, they are intrinsically faint, making their study and density profile determination, quite difficult. However, Milky Way (MW) dSphs are sufficiently nearby for detailed observing of their kinematics, which has supported the strong DM presence given the amplitude and radial profiles of their velocity dispersion (Hammer et al., 2018). Large DM halos are assumed around these systems, given their proximity to the MW, lying rather near to their pericentre ($\lesssim$ 20 kpc), while still keeping a spheroidal morphology (Fritz et al., 2018). Consequently, dSphs not only can help in understanding the physics behind galaxy formation, but also serve as probes into the nature of DM.

Since the 1930s we have been trying to elucidate the nature of this exotic obscure matter (Zwicky, 1937). For quite some years now, it has been clear it has to be non-baryonic matter if it was to fit in the Big Bang open universe inflationary scenario. By shifting the focus towards non-baryonic matter, particle physics became the place to look for answers considering likely candidates had already been independently developed to solve issues in the Standard Model of quantum field theory. However, the exact particle that would fit this exotic matter in question, is a topic still largely debated (Freese, 2017). The particle nature of DM has a direct influence on non-linear cosmological structure, such as halos. In fact, DM candidates have been categorised based on their effects on structure formation. Hot DM, previously mentioned, remains relativistic until quite late in the Universe's evolution, smoothing perturbations on super-galactic scales; Warm DM, has smaller initial velocities meaning it becomes non-

relativistic earlier, suppressing perturbation on galactic scales; lastly Cold DM almost does not have thermal velocity, thus it doesn't suppress structure formation (Bullock & Boylan-Kolchin, 2017). Of this three, Cold Dark Matter (CDM) has been reigning as the favourite because of the match with large structure formation, yet doubts about the accuracy of this choice emerge when looking at sub-galactic scales (Bode et al., 2001).

It must be acknowledged that the current cosmology model, known as the ΛCDM, has had many successes. It provided a confluence between particle physics and astrophysics, and was the culmination of years of work across both fields, describing accurately the Universe's large scale structure formation and evolution, its early state and the proportion of its content in matter and energy. All of it backed by observational data, like the measurements from the Cosmic Microwave Background, a relic from the Big Bang (Trimble, 1987; de Swart et al., 2017; Del Popolo & Le Delliou, 2021). However, from the moment N-body simulations were able to resolve the formation at smaller scales, a number of issues arose (Flores & Primack, 1994; Moore et al., 1999; Klypin et al., 1999). One of these problems being the cusp-core, the topic of this thesis. The possible solutions to such contradictions can be divided in three groups: data errors; interaction between standard matter and DM; and the most interesting, and perhaps daring, would be to change our theories around the nature of DM (Read et al., 2018). The latest generation of highly accurate kinematic data has shifted the focus to the latter two options (Battaglia et al., 2022). Both the improvement on observational data and increase in our computer power, make unavoidable the tension with the current model becomes (Frenk & White, 2012). Nonetheless, there is a general reticence to modify the ΛCDM, given its great description at other scales, unless the rest of possibilities to explain these contradictions between theory and observations, are exhausted (Bullock & Boylan-Kolchin, 2017).

Considering everything that has been mentioned above about the old cusp-core debate and its numerous ramifications, from galactic scales to particles nature, there is no doubt about the complexity and depth of such topic. Hence the aim of this project was not to solve the issue between cusp and core, but rather take them both for their face value and expose them to the same potential to pinpoint clear differences on how tidal disruption affects each distribution. The simulation was ran with different truncated Navarro-Frenck-White (NFW) profiles (Navarro et al., 1996b) separately, to later compare the correspondent results when evolving the artificial systems over time. Thus, our goal was to aid in the study of how the distribution of dSphs would be affected by their current orbits, without further as-

sumptions of the origin or evolution of such distribution. This would have a double purpose on surveying the inherent nature of DM given the different kinematic responses that could be observed, thanks to the little standard matter present in dSphs.

The way this paper is structured is as follows: Chapter 2 provides background on the cusp-core problem, and the cosmological theories behind as well as possible DM candidates. Chapter 3 covers the methodology followed to build up the N-body simulation of a dSph, from how it was populated according to their respective density distribution, to their implementation on an orbit around a galactic potential. Chapter 4 is where the final results and analysis are exhibited, as well as bringing real data into the discussion. Finally, Chapter 5 draws the conclusion, and possible future applications of this project results. In the appendix, some additional plots are presented.

2 Background

In this chapter we will be reviewing the discovery and search for Dark Matter, and how the possible candidates for its nature affect sub-galactic structure formation, specifically focusing on halo formation for the sake of this thesis.

2.1 Discovery of and evidence for DM

Dark matter nature remains a mystery, yet a crucial element to explain the dynamics and evolution of our Universe. According to the current cosmological model, it accounts for around 26% of the matter in the Universe, while standard baryonic matter stands for only 5% (Freese, 2017). Hence, it has been an urgency to tackle the obscure matter and its properties in order to better understand our Universe. This search has been going since the initial proposition for dark matter as a plausible theory in the 1970s. Despite Zwicky's early claim's in the 1930s for the need of additional matter to explain the relative high speeds of galaxies compared to their luminous mass (Zwicky, 1937); DM wasn't the first answer to the issue. Many symposiums took place in the 1960s after new astronomical surveys showed disparity between galactic masses and their velocity (Shane & Wirtanen, 1954; Abell, 1959), yet DM was just one of many options brought to the table. The rise of radio astronomy in the 1960s revealed the flat rotation curves of galaxies (Rubin & Ford, 1970), instead of dropping as luminous matter decreased at outer radii. These observations of galaxies high dispersion velocities and flat rotation curves are regarded nowadays as the first experimental evidence of DM. However, their correlation wasn't noticed until the steady-state picture was dropped, envisioning instead a evolution of the Universe. Such readjustment of the view of the universe was precipitated by the discovery of quasars at great distances along with the measurement of the Cosmic Microwave Background (CMB) radiation predicted by Big Bang theories (de Swart et al., 2017). This new evolution perspective provided a link to the observed phenomena with the first papers on DM theory coming out in the 1970s (Ostriker et al., 1974; Einasto et al., 1974). Shortly after, DM was consolidated as the main theory being key to in the birth and evolution of the Universe through inflation and its influence on structure formation (Trimble, 1987).

The different trials at detecting DM have been various during the decades. The first searches in the 1980s focused on baryonic matter with faint stars, brown dwarfs, white dwarfs and neutron stars as the possible candidates. These were labelled as Massive Compact Halo Objects, because they were

expected to be highly dense in galactic halos to explain the flat rotation curves. By the end of the 1990s the Hubble Space Telescope data had determined their percentages to be too low to account for all the missing mass (Freese et al., 2000; Alcock et al., 2000) . From there, the focus was redirected towards non-baryonic matter, manoeuvre that brought particle physics into the picture. Many suitable particles of non-baryonic nature had been developed to tackle issues within the Standard Model of quantum field theory (Boyarsky et al., 2019). Hence, the pursuit of DM candidates is one of the cornerstones in the search for physics beyond the standard model, standing in the frontier between particle physics, astrophysics and cosmology (Bertone & Hooper, 2018). The joint efforts from both fields built a symbiotic relation in which astrophysical observations would put constraints on the theoretical models from particle physics redirecting future theories (Bertone et al., 2005). Early on the search, neutrinos had appeared as a simple choice given their proven existence and their great abundance which almost matches the number density of photons (Muñoz, 2004). Yet when N-body simulations began to be utilised in the 1980s to replicate structure formation of the Universe (White et al., 1983), the model ran into problems because of its 'hot' nature. The 'hot' nature referred to how neutrinos still had relativistic speed at the time structures were being formed according to the Big Bang model. As a result, a 'top-bottom' scenario would occur in which galaxies would origin from the fragmentation of larger structures. This was in complete disagreement with observations, that had exposed galaxies to be older than superclusters (Taoso et al., 2008).

To accommodate the results from simulations and observations, a 'bottom-up' formation scenario was suggested, where smaller structures would merge to form larger ones. This entitled for DM to be non-relativistic during the formation period of the Universe, hence branded as Cold DM (CDM). The matches this model provided at large scales quickly positioned it as the standard theory for DM, experimental searches being mainly focused on CDM candidates since (Blumenthal et al., 1984; Davis et al., 1985; Drukier et al., 1986). The favourites within such theories have been the Weakly Interacting Massive Particles (WIMPs). Their popularity comes from what is known as the 'WIMP miracle', referring to how their predicted abundance as a 'thermal relic' from the early Universe would be consistent with the required DM abundance, if they were to exist (Feng, 2010). In addition, they arise from multiple particle physics theories, as the Super Symmetry (SUSY) model which assigns partners to the current Standard Model particles to hold them at a correct value (Freese, 2017), hence also solving issues in

the particles' field. The efforts to detect WIMPs have been extensive covering both direct and indirect approaches. The direct methods aimed at picking up signatures of DM scattering off standard matter, hoping to detect the "wind" of WIMPs from Earth. If WIMPs were to be clustered in galactic halos as expected from DM gravitational effects, the Earth's motion around the Sun would cause an average relative velocity with respect to them. Many laboratories have been built underground to filter cosmic rays in order to pick up such signal, yet only the DAMA experiment in Italy has had a positive signal (Bernabei et al., 2018) until this date. The signal interpretation is an ongoing debate due to the lack of confirmation from other experiments, thus new experiments using the same material in the detector as DAMA are being set in motion to try at replicating the results (Amaré et al., 2021). Similarly, the indirect approaches which are aimed at detecting WIMPs annihilation or decay from astrophysical sources like dwarf galaxies, remain inconclusive (Arcadi et al., 2018; Klasen et al., 2015).

The lack of success at detecting WIMPs has now spanned over two decades, reason why the focus has started to shift towards other theorised candidates. Among the many options sterile neutrinos have resurfaced as likely candidates. While also predicted by particle theories beyond the Standard Model, one of their main pulls is their 'warm' DM nature. This means they would have relativistic velocities at the start as in the Hot DM picture, but they do not cluster, allowing them to stream freely (Boyarsky et al., 2019). In following sections it will be further explained how the Warm DM model seems so promising to fit the observational data better than the standard Cold DM.

2.2 Challenges to CDM from N-body simulations

As mentioned previously, the CDM paradigm took front stand in the 1980s due to great matches with the evidence from large-scale galaxy clustering, as well as the Cosmic Microwave measurements among other data (Peebles, 1982; Blumenthal et al., 1984). Nonetheless, with the implementation of N-body simulations in cosmological studies during the 1990s, challenges to the CDM model arose immediately regarding small-scale predictions (Flores & Primack, 1994; Moore et al., 1999; Klypin et al., 1999). Below the main problems are exhibited, especially highlighting the cusp-core debate studied on this thesis.

2.2.1 Missing Satellites

When following hierarchical models as CDM, smaller galaxies are expected to collapse earlier when the density of the Universe was higher. Therefore, the satellites of our Milky Way (MW) galaxy would have

been formed before the MW structure was assembled. As a result, some of the satellites would have been accreted by the MW while others would have been able to survive (Klypin et al., 1999). The issue appears when comparing the number of predicted satellites to survive til today in CDM simulations of MW formation, with the observed satellites orbiting our galaxy. The problem is quite severe since only around ~ 50 satellite galaxies with enough mass to support molecular cooling, compared to $\sim$1000 dark subhalos which a large galaxy could hold (Bullock & Boylan-Kolchin, 2017). The difference between predictions and observations has been slightly softened by new discoveries of ultra-faint dwarf satellites (Tollerud et al., 2008; Kuhlen et al., 2012), but it seems unlikely that there would be still thousands of dwarf galaxies undiscovered within the virial radius of the MW. Another solution would be that galaxy formation becomes increasingly inefficient as halo mass drops, hence the smallest halos wouldn't have formed stars (Bullock & Boylan-Kolchin, 2017).

2.2.2 Cusp-Core

The second problem, and the most relevant to this thesis, is the cusp-core controversy. The issue comes from central regions of low-mass galaxies, meaning DM dominated, being less dense and less cuspy than predicted from CDM simulations (Flores & Primack, 1994). According to the CDM scenario DM halos should rise steeply at small radii $\rho(r) \propto r^{-\gamma}$ with $\gamma \simeq 0.8 - 1.4$ (Navarro et al., 2010); hence, a cusp density profile. However, the kinematic measurements from low surface brightness galaxies (e.g. dwarf galaxies), fit better constant density cores ($\gamma \simeq 0 - 0.5$) (Bullock & Boylan-Kolchin, 2017). The many solutions proposed can be divided in three categories, the most straight forward being data problems, either due to wrong measurements (de Blok, 2010) or inaccurate modelling of the motion of dwarfs among other possibilities (Valenzuela et al., 2007). The second category would be considering possible interactions between baryonic and DM matter, aiming to solve the issue without having to modify the CDM paradigm. Hydrodynamical simulations have shown that supernovae explosions could heat up the gas in DM halos driving it to larger distances, hence, multiple bursts could grind the cusp profile into a core (Navarro et al., 1996a; Read & Gilmore, 2005; Pawlowski, 2021). This transformation of the density profile by stellar feedback, would only be possible if there was enough amount of mass to drive such process, which has been determined to be above $10^6\ M_{odot}$ (Bullock & Boylan-Kolchin, 2017). However, at least half of the satellites orbiting the MW are below such mass, thus leaving their low central densities unexplained. On the other hand, interactions between these satellites and the MW could also act as

feedback reducing the central density of satellites (Zolotov et al., 2012; Arraki et al., 2014). In specific, the tidal stripping effects regarding such matter were of particular interest in this project.

The possible evolution between cusp and core profiles appears to be required if were to use baryonic interactions as the solution to these challenges. Since, depending on the baryonic phenomena, one of the profiles is favoured above the other. For instance, the violent relaxation, expulsion of leftover star-forming gas, that star clusters undergo during their evolution would require of a cuspy DM halo for the system to survive such process while still being gravitationally bound nowadays (Parmentier, 2009). On the other hand, when looking at dynamical friction, the drag force between a massive object moving within a sea of lighter field stars, if halos were to have cuspy profiles, globular clusters would sink to their centre while core profiles would be able to suppress such effect (Petts et al., 2016; Contenta et al., 2018). Also, core profiles appear to be more susceptible to undergo accretion, which could a way to tackle the missing satellites (Miholics et al., 2014). It has been recently theorised that a regenartion of a core into a cusp profile could also be possible when considering late minor mergers (Laporte & Penarrubia, 2015). As promising as possible transformations between cusp and core theories might sound, it is fair to say that is still quite a feat to develop a transformation theory which satisfies all these observations, while keeping it within the constraints of the CDM scenario.

The last category of solutions to this issue, and perhaps more enticing, would be modifying the nature of DM itself. Among the possible candidates the ones we will be discussing are: Warm DM (Bode et al., 2001; Dalcanton & Hogan, 2001; Schneider et al., 2017), Self Interacting DM (Spergel & Steinhardt, 2000; Rocha et al., 2013; Elbert et al., 2015) and 'fuzzy' DM (Hu et al., 2000; Pils & Rindler-Daller, 2022). Their fitting characteristics will be further explained ins following Section 2.3.

2.2.3 Too-Big-to-Fail

This last concern is a confluence of the first two problems. Considering the observations, satellites orbiting the MW are less dense than predictions from CDM. Thus, allegedly according to the CDM model, there would be satellites of higher density than the ones observed still missing. However, if they were to exist the solution proposed in subsection 2.2.1 would not hold, since these missing satellites would be too big to fail at forming stars (Bullock & Boylan-Kolchin, 2017).

2.3 Nature of DM & subgalactic structure formation

The particle nature of DM has an effect in the cosmological perturbation spectrum, affecting the non-linear regime of structure formation as galaxy halos. The dSphs halos are perfect laboratories for this study considering they are DM dominated and their shallow potential wells are more sensitive to energetic feedback allowing to provide constraints (Read et al., 2016). Especially, looking at small-scale structure formation maximises the difference between DM models, as the suppression on structure formation depending on the particle nature becomes more evident at subgalactic scales (Bullock & Boylan-Kolchin, 2017). It's worth noticing that all these models are able to solve the previously mentioned subgalactic problems without the need of baryonic feedback. Below, the favourable arguments of alternative candidates of DM from the standard CDM are briefly exhibited:

2.3.1 WDM

Warm DM appears as one of the simplest modifications, being a middle ground between the top-bottom Hot DM scenario, which was discarded at large scales, and the bottom-up standard CDM challenged at smaller scales. Considering the high velocity of WDM particles in the early Universe, a larger free streaming length would be achieved compared to CDM, thus suppressing small perturbations. As a result, in a hierarchical formation scenario far fewer small-scale DM halos would be formed, tackling the missing satellites issue (Bode et al., 2001). The effect of power suppression decreases the number of subhalos because it delays the assembly of halos for a particular mass, compared to the case without such suppression (e.g. CDM). This can be observed in fig.1 were its apparent fewer structures have had time to be formed in the WDM than in the CDM case. The delay forming halos would result in lower central densities, solving the the Too-Big-To-Fail (TBTF) problem (Anderhalden et al., 2013).

2.3.2 SIDM

The standard CDM is regarded as collisionless, only considering gravitational interactions in which individual particles interactions are negligible in comparison to the large-scale effect from the gravitational potential. Instead, Self-interacting DM models investigate the possibility that DM particles actually would have strong self-interactions, hence also called collisional DM (Carlson et al., 1992; Spergel & Steinhardt, 2000). SIDM would retain the large-scale matches of CDM, as well as the distribution of

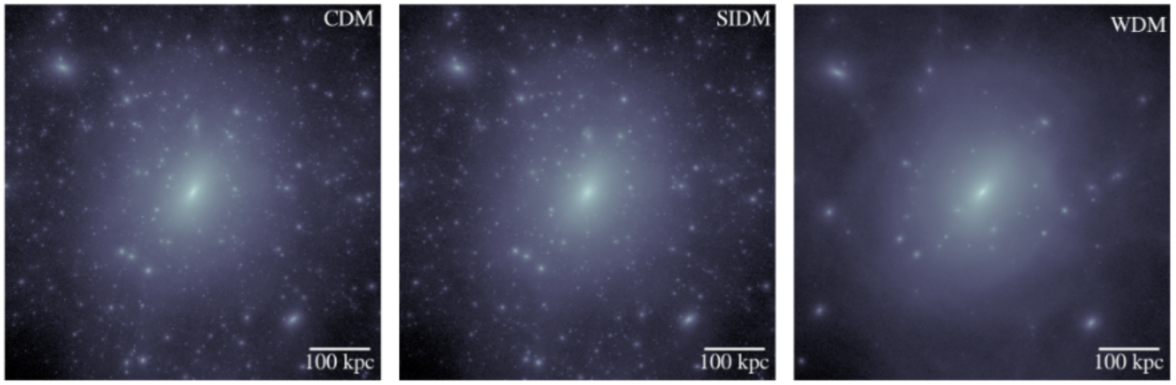

Figure 1: The images show the same MW-size DM halo simulated with CDM, SIDM and WDM, taken from Bullock & Boylan-Kolchin (2017).

subhalos while modifying their internal structure. The self-interaction would enable isothermal cores to be formed, rather than cuspy profiles, easing the cusp-core and TBTF issues (Pawlowski, 2021). This positions it in a favourable spot, middle way between the CDM and the WDM models (fig.1), retaining the good matches at large scales from CDM, while also tackling the small-scale challenges (Frenk & White, 2012).

2.3.3 Fuzzy DM

Fuzzy DM is a model aims at conserving the standard CDM model, also known as Scalar Field DM (SFDM), it postulates that DM would be made of ultra-light bosons, which condensed into their ground state can be described by a single scalar field. If the particles are ultra-light, then their wave nature would manifest even on astrophysical scales, allowing DM halos to be stable thanks to the uncertainty principle in wave mechanics (Hu et al., 2000). This model has become popular due to its ability to predict galactic cores, unlike the CDM regime. Another interesting feature in tackling the small-scale problems, is how the length scale at which they start to suppress structure formation is relatively large given its broad definition particle wise (Pils & Rindler-Daller, 2022).

3 N-body simulations

Cosmological N-body simulations have been essential for the progress of our understanding on large-scale structure formation in the Universe. The increasing numerical resolution has allowed us to investigate non-linear scales as the gravitational collapse of galaxy halos where analytical approximations fail (Gao et al., 2012). In fact, it has been shown how the models for DM halos inferred by N-body simulations, as it is the case of the NFW used in this project, fit really well the direct measurements of the distribution of DM matter in galaxies obtained from gravitational lensing (Okabe et al., 2013). Furthermore, accurate dynamical mass measurements have been obtained in past studies using N-body simulations (González-Samaniego et al., 2017), despite taking strong assumptions as isotropy, spherical symmetry and non-rotation of the simulated dwarf galaxies . Therefore, we used such approximations in our N-body program, especially since dwarfs spheroidals (dSph) show little rotation and their morphology is quite spherical (Wheeler et al., 2017). Something to keep in mind is that in collisionless N-body simulations, the point-particles are phase-space representations, making it possible to actually use less than the actual number of DM particles.

This chapter will outline the numerical setup of the N-body simulations used to follow the tidal evolution of our dSph model in the gravitational potential of the MW.

3.1 Generating artificial cluster

As our aim is to be able to simulate the evolution of a cluster, the first step is to generate a stable system which we could later disturb adding external factors. Thus, we started from an 'ideal' cluster which would be in equilibrium, is isotropic and homogeneous. Galaxies can be seen as collisionless systems, considering the long rages forces dominate over the short range interactions that could arise in such large structures. In fact, even if the there was to be a close encounter this one would be considered 'weak', meaning they would only create a tiny perturbation to the motion of the stars which isn't substantial and can be neglected from our zoomed out perspective. Especially since the relaxation time for galaxies, which is time taken for a galaxy's velocity to be changed significantly by two-body interactions, is very long, longer than the age of the Universe.

Considering all the above statements, one can apply the Collisionless Boltzmann Equation:

$$\frac{\partial f}{\partial t} + \sum_{i=1}^{3} \left(\frac{dx_i}{dt} \frac{\partial f}{\partial x_i} + \frac{dv_i}{dt} \frac{\partial f}{\partial v_i} \right) \equiv \frac{df}{dt} = 0$$

So f represents the probability of two galaxies colliding, and it provides a relationship between the density of stars in phase space for a galaxy with position x, stellar velocity v and time t. It should be noted that density in phase space f does not change with time for a test particle.

Any steady-state solution of the Collisionless Boltzmann equation depends on the phase-space coordinates only through integrals of the motion in the galaxy's potential, and any function of the integrals yields a steady-state solution. Hence, when using a potential which doesn't change over time, as it is the case of a cluster in equilibrium, then we can solve the distribution function in terms of the integrals of motion. This is known as the Jeans Theorem.

If now we assume isotropy, the distribution function would shift to the form $f(r, v)$, reducing the 6 dimensions of the original equation to just 2 (radial and velocity). Furthermore, this can be more simplified by considering an ergodic distribution function ($f(E)$), meaning we assume the equations describing the dynamics of our system won't contain random perturbations, in agreement with in equilibrium scenario. Thus, applying the Jeans Theorem to this isotropic spherical model, any function of the form:

$$f(E) = f\left(\frac{1}{2}v^2 + \Phi(r)\right)$$

would also be a solution to the time-independent Collisionless Boltzmann equation. To have a self-consistent solution, the gravitational field needs to be related to the density by Poisson's equation, yielding:

$$\frac{1}{r^2}\frac{d}{dr}\left(r^2 \frac{d\Phi}{dr}\right) = -4\pi G\rho$$

Then, if we assume all stars have the same mass within the spherical isotropic system, the density could be express as:

$$\rho(r) = \iiint d^3\mathbf{v} f = \int_0^{\sqrt{2\Phi}} \mathrm{d}v v^2 4\pi f(E)$$

where the upper limit stands for the escape velocity at radius r. Since the potential is a monotonic function of r in this scenario, then we can change the variable from r to Φ:

$$\rho(\Phi) = 4\sqrt{2\pi} \int_{\Phi}^{0} \mathrm{dE}\sqrt{E - \Phi} f(E)$$

with the upper limit referencing to the point where particles wouldn't be bound anymore to the gravitational system. When derivating with respect to the potential, we obtain:

$$\frac{d\rho(\Phi)}{d\Phi} = -\sqrt{8}\pi \int_{\Phi}^{0} \mathrm{dE} \frac{1}{\sqrt{E-\Phi}} f(E)$$

This it's known as the Abel integral equation, which solution for the energy distribution function, is the Eddington's inversion formula:

$$f(E) = \frac{1}{\sqrt{8}\pi^2} \frac{d}{dE} \int_{E}^{0} \mathrm{d}\Phi \frac{1}{\sqrt{V-E}} \frac{d\rho(\Phi)}{d\Phi} \tag{1}$$

This equation lets us obtain the energy distribution for a cluster given the potential $\Phi(r)$ and the density distribution $\rho(r)$. Thus, we could build a program in which you would just enter a radius vector and density profile, and an energy distribution could be inferred, since the solution to this equation is unique. Yet one needs to be careful when selecting the variables, since it's not assured the solution would be physical ($f(E) > 0$) (Weinberg, 2020).

In order to implement the equation, of the first things to be tackled was the singularity points at the maximum of the potential. To do so, a change of variables was performed introducing a new variable $Q = \sqrt{\Phi - E}$. According to this substitution, the limits of integration become 0 for the lower one, where all the energy comes from the potential, and $\sqrt{E}$ for the upper one where the potential reaches zero at the limit of the cluster.

Provided the density and spatial coordinates, the accumulated mass function could be calculated as follows:

$$M(r) = 4\pi \int_{0}^{r} \rho(r') r'^2 \mathrm{dr'} \tag{2}$$

Using the above expression we could compute the gravitational force experienced at certain r within the cluster. Then, from the gravitational force values, the potential could be obtained by integrating over r. The issue was that it had to be normalised so that at large distances it would approach zero as expected from a gravitational bounded system. To such end, the maximum value within the potential array, meaning the maximum of potential, as well as the value obtained for maximum potential when using the analytical expression for potential, which differed from the value obtained by numerical integration, were subtracted from all the values in the array. This worked well, resulting in a potential with negative values that decreased towards zero as the limit of the cluster was reached. However, there were some issues with the innermost values at small r. To tackle this problem, the initial values of the potential were

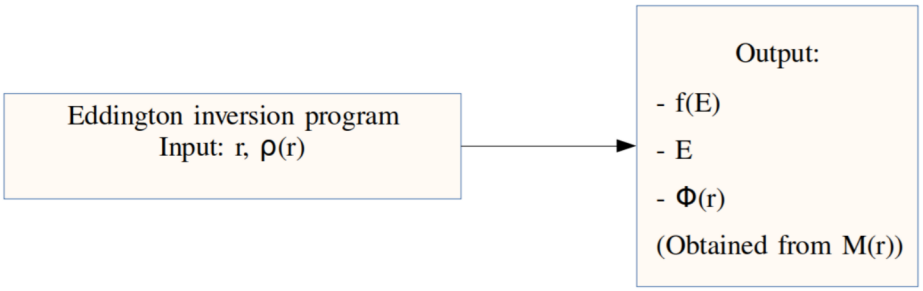

Figure 2: Flow map of the function built to estimate the energy distribution based on the Eddington Inversion Formula.

computed by assuming a spherical volume (isotropic) at the inner part of the cluster, which multiplied by the density could be plugged in as the mass variable in the expression for the potential. These values also had to be normalised so the parabola would be placed at the bottom of the potential.

$$\phi_{r\to 0} = \int F \mathrm{dr}$$

$$\phi_{r\to 0} = \frac{2\pi G \rho_0 r^2}{3} + \kappa$$

in which κ is the constant that we need to tweak to place the parabola at the right spot, specifically at the maximum value of the potential, thus its values in our case was:

$$\kappa = -\left[\frac{2\pi G \rho(r_{max}) r_{max}^2}{3} - \phi(r_{max})\right]$$

Taking all the above in consideration, a function was build so that given the arrays for r and $\rho(r)$, it would return the $\Phi(r)$, E and the energy distribution $f(E)$ (fig.2). Numerical methods were applied to estimate values of the derivatives (finite difference) and integral (cumulative sum). In order to test its accuracy, a simple homogeneous model was used, the Plummer sphere (Plummer, 1911). This model has been used often in N-body simulations (Shukirgaliyev et al., 2021; Read et al., 2018; Contenta et al., 2018), and despite its simplicity, it describes quite well globular clusters. The Plummer model density function is defined as follows:

$$\rho(r) = \frac{3 \cdot M \cdot a^2}{4\pi} \left(a^2 + r^2\right)^{-\frac{5}{2}} \tag{3}$$

where M is the mass of the gravitationally bound system in question, so in our case the mass of a dSph is of the order of $10^5 - 10^9 M_\odot$, while the scale size a used was chosen to be 10, a unitless parameter (González-Samaniego et al., 2017). The results can be seen in fig.3, where we use $M = 10^7\ M_\odot$, and the

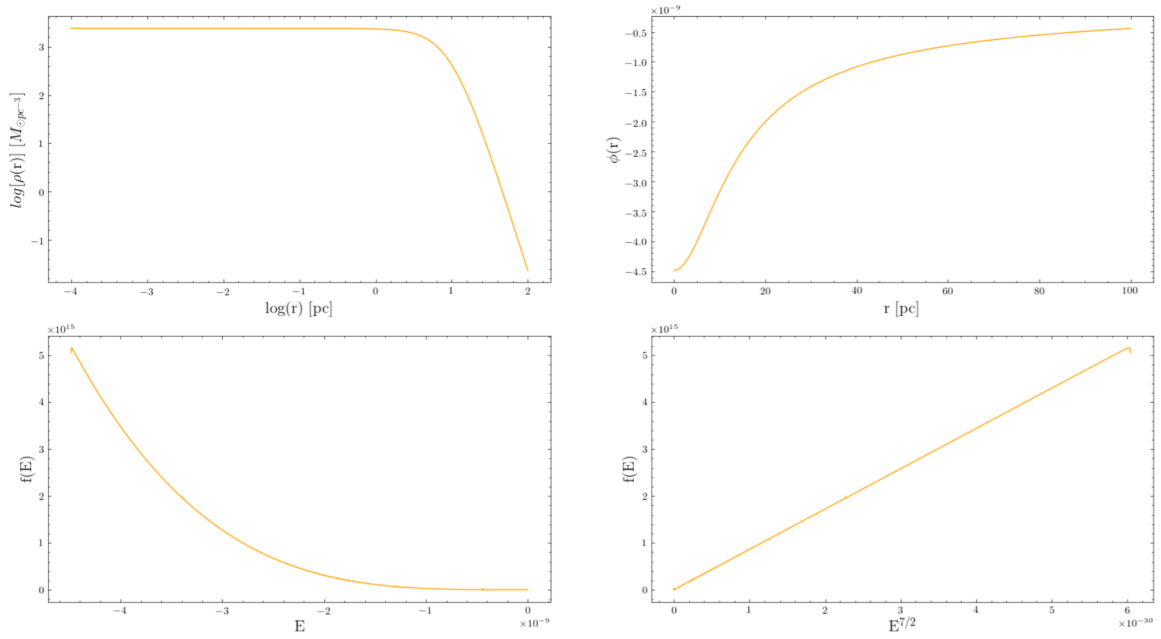

Figure 3: Various plots from the Plummer model using a mass of the order of 10^7 $M_\odot$ and using the Eddington inversion program to infer the energy distribution.

program accuracy it's visible on the right bottom corner graph in which we can see the energy distribution obtained, $f(E)$, is directly proportional to $E^{7/2}$ as expected from Plummer's analytical form.

After making sure the Eddington inversion formula was well implemented, we proceeded to use a more accurate profile for our halo. This was the Navarro-Frenk-White (NFW) profile (Navarro et al., 1996a), which provides a better description of the density distribution for a DM halo following the CDM paradigm. The form of such model is as follows:

$$\rho_{NFW}(r) = \rho_0 \left(\frac{r}{r_s}\right)^{-1} \left(1 + \frac{r}{r_s}\right)^{-2} \tag{4}$$

in which r_s is the scale length, and the central density ρ_0 is defined by:

$$\rho_0 = \rho_{crit} \Delta c^3 g_c / 3$$

$$g_c = \frac{1}{log(1+c) - \frac{c}{1+c}}$$

where c is the dimensionless concentration parameter, and in our simulation was selected to be 14 as in Read et al. (2018). While Δ=200 is the over-density parameter, and ρ_{crit}=136.05 $M_\odot kpc^{-3}$ is the critical density of the Universe at redshift $z = 0$. Thus, the enclosed mass for the NFW profile would be obtained from the 'virial' mass M_{200}, which is the mass enclosed within the 'virial' radius. This so

called 'virial' limit was drawn when the NFW was formulated by Navarro et al. (1996a) using N-body simulations, and this point was reached when the clumps which merged following the CDM structure formation picture, made a halo centre reaching an overdensity of 200. Therefore, the mean enclosed density is equal to Δ x ρ_{crit} at this 'virial' limit, and the total mass of the halo would be:

$$M_{NFW}(r) = M_{200} g_c \left[ln\left(1 + \frac{r}{r_s}\right) - \frac{r}{r_s}\left(1 + \frac{r}{r_s}\right)^{-1} \right] \tag{5}$$

Although in tune with theoretical predictions, this model doesn't quite cut it when looking at experimental measurements of dSph. Observations from various dwarf galaxies favour a central dark matter core over cusps, or at least something in between (Read et al., 2016). These dark matter cores are not predicted by collisionless CDM structure formation simulations, which could mean new physics, yet first the possible known mechanisms that could provoke it would have to be discarded. It would be possible to explain a cusp to core transformation within our current physical understanding, if repeated star formation bursts were to happen, a cusp could be grind down to a core. For such process to occur though, the mass scale of the galaxy would have to be sufficient to reach the energy needed to unbind the cusp. However, such estimation is not an easy task since many assumptions are taken as the radial dark matter profile or the size of the core. There is even hypothesis about core to cusp transformation from late minor mergers (Laporte & Penarrubia, 2015).

Rather than diving in the possible transformation processes, the focus of this project was to find the differences between the two models. Since, if morphological clear differences were to be observed, this could add to the debate given more clues on how to differentiate the profile when observing dwarves, or what most likely was their starting point distribution before suffering tidal disruptions. Our simulations didn't account for the multiple stellar processes said to be precursors for the transformations, hence allowing our results to be applied in a general way to any of those scenarios.

In Read et al. (2016) they proposed a truncated NFW density profile which encapsulates both the cusp and core models, as seen below:

$$\rho_{cNFW}(r) = f^n \rho_{NFW} + \frac{n f^{n-1}(1 - f^2)}{4\pi r^2 r_c} M_{NFW} \tag{6}$$

$$f^n = \left[tanh\left(\frac{r}{r_c}\right) \right]^n$$

where the n controls how shallow the core becomes, with $n = 0$ corresponding to the cusp model, and

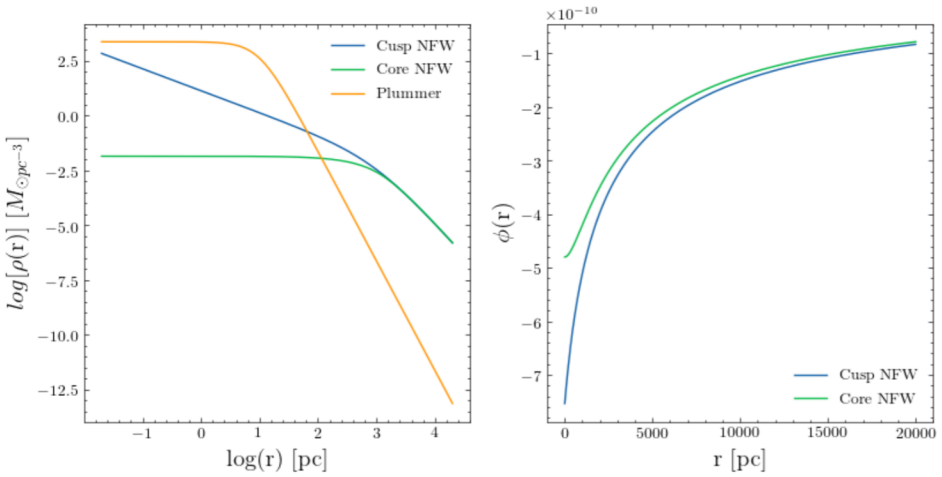

Figure 4: On the left density distribution of the NFW models vs the previous Plummer one where $M_{Plummer} = M_{200} = 10^7\ M_\odot$ and $r_s = r_c = 1$ kpc. On the right comparison of cusp vs core potential distributions.

$n = 1$ to the core one. A comparison of how these distributions compare to the previous spherical Plummer model can be seen in fig.4.

3.2 Populate phase-space with N-body particles

Once we were able to generate the correct energy distribution, the next step was to populate the artificial cluster following the given profile. To do such thing, we employed a rejection sampling method. The principle behind it, is that one can perform a uniformly random sampling of the two-dimensional Cartesian graphs, keeping only the samples in the region under the graph of its density function. This way, we could infer the position values from the mass accumulated function and the velocities from the phase-space function.

3.2.1 Spatial distribution

The spatial placing of the number N of particles chose for a simulation would be based on the $\rho(r)$ given as input. From the density distribution, one could calculate the accumulated mass function (eq.2). After normalising the function, it could be inverted allowing us to set an interval within which we could draw random values, while still making sure the distribution $\rho(r)$ was followed when put all together.

From the accumulated mass function (eq.2), it was also possible to obtain the total mass of the

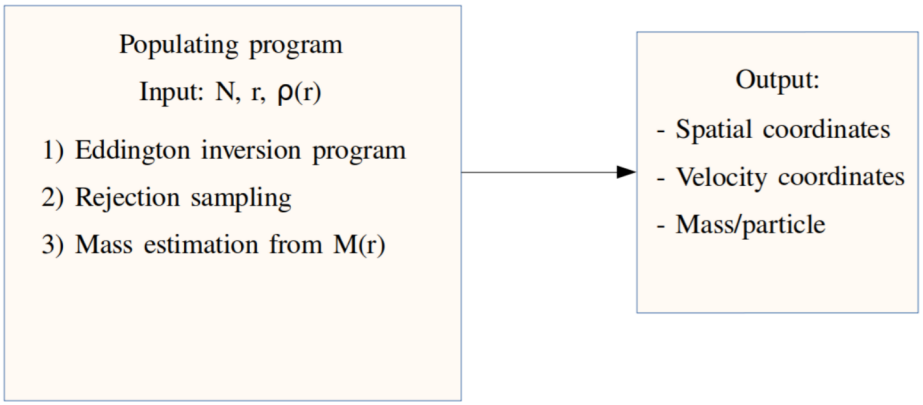

Figure 5: Flow map of the function built to generate and populate the system.

gravitational bound system. If we consider the maximum value from our mass function, then the total mass of the system given it's a spherically symetric and isotropic one would be:

$$M_T = 4\pi M(r)_{max} \tag{7}$$

3.2.2 Velocity distribution

To obtain the velocity associated to the randomised coordinates, a similar process was used. This time the interval from which to pick values was set by the phase-space cumulative function:

$$F(v,r) = 4\pi \int_{\Phi(r_0)}^{0} f\left(\Phi(r) + \frac{v^2}{2}\right) v^2 \mathrm{dv}$$

The difference compared to eq.2 is that the lower bound of this integral changes at different r, hence the geometric factor v^2 needed to be calculated at each r. At this point, we were able to generate an isotropic artificial cluster in equilibrium just by providing: an initial r vector, of sensible size considering the average size of dwarf galaxies; a density distribution $\rho(r)$, according to the desired model (e.g. Plummer); and the number of particles N within the cluster, which must be noted doesn't correspond to the number of stars rather to groups of them. Once again the efficiency of the program was tested first with the Plummer model, giving the isotropic spherical symmetric distribution expected, as seen in fig.6.

3.3 Evolve through time

The next step was to evolve this cluster over time, which was achieved by employing REBOUND, an N-body integrator package (Rein & Liu, 2012a). REBOUND is quite an adaptable package, which made

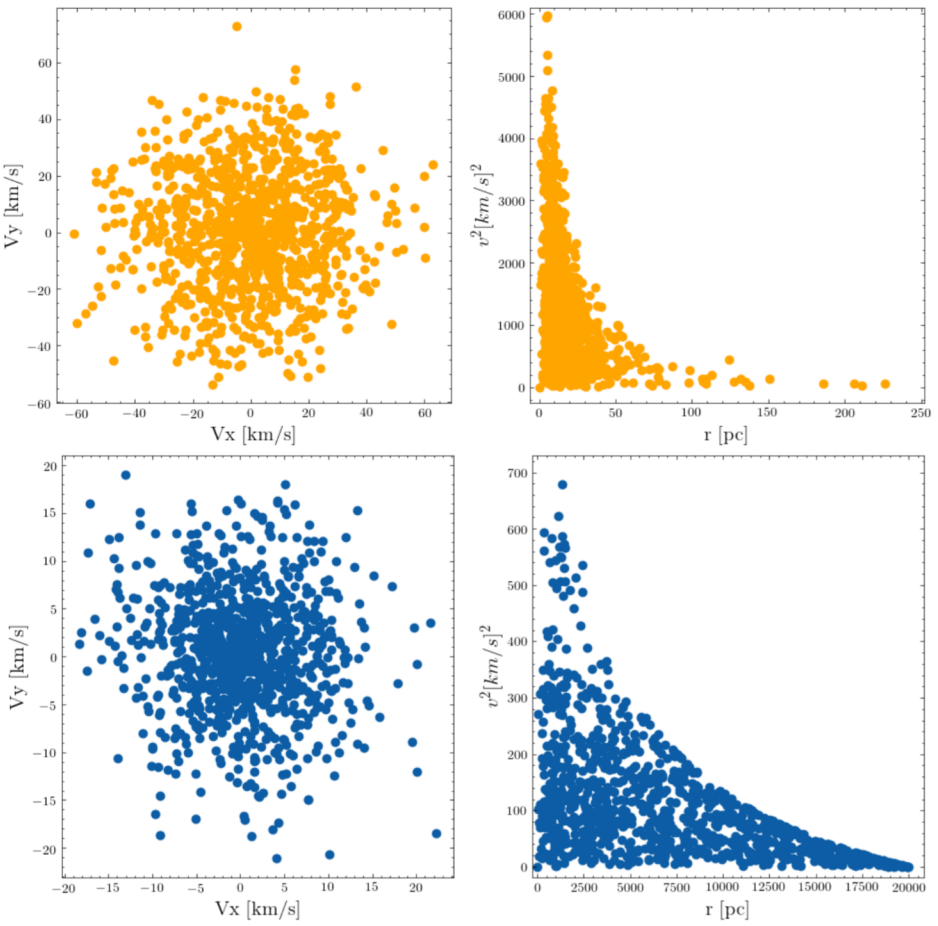

Figure 6: First row: Plummer velocity phase-space distribution results when using the rejection sampling based code for $M = 10^7\ M_\odot$. Second row: Same graphs as first row, but using the cuspy NFW profile instead, for a $M_{200} = 10^7\ M_\odot$ and $r_s = 1$ kpc.

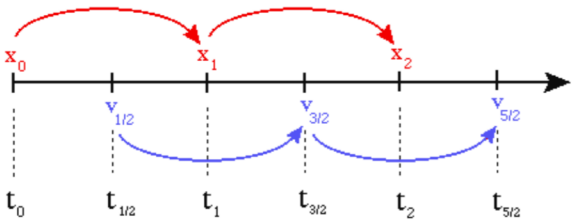

Figure 7: Visual representation of the leapfrog integration method.

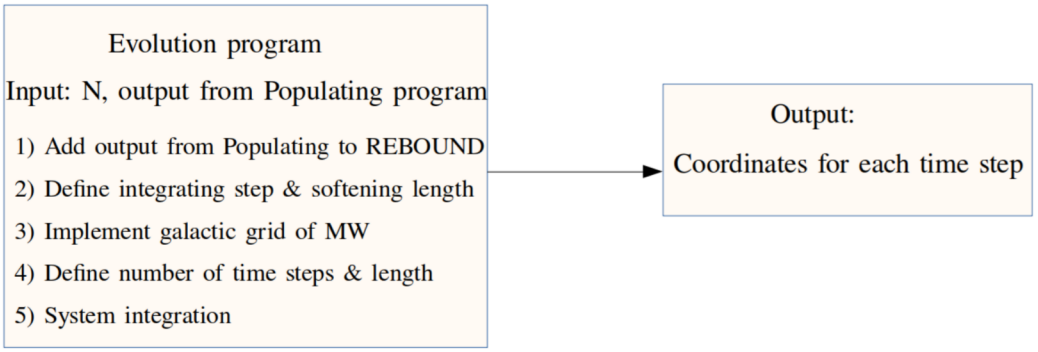

Figure 8: Flow map of the function built to integrate the system over time using the REBOUND package.

possible evolving our collisionless simulation using a symplectic integrator. Symplectic integrators give a numerical solution to Hamilton's equations, allowing to solve the dynamics of the system in question. In particular, the LEAPFROG integrator was the one used in this simulation since we were considering classical mechanics dynamics. This is a second-order method which updates positions and velocities at staggered time points in a way that the 'leapfrog' over one another as seen in fig.7 (McMillan, 2022). The step taken by LEAPFROG is constant throughout the integration of the simulation, which at first was picked to be 10^4 yr, but was increased to 1 Myr, since an average star moves barely a few arcseconds per year and this way the program would be quicker. Then, the number of steps was selected thinking of having enough snapshots of the evolution to witness possible perturbations, and to cover enough time to follow the orbit around the MW centre. After many trials, 20 steps of 10^8 years was selected as a good fit, meaning a 2 Gyr long simulation.

A variable that was needed in during these simulations was the softening length. At small separations the gravitational attractions between the particles of the simulation can become large, diverging and going against the smooth collisionless principle the simulation was built on. In order to tackle this issue, the gravitational interaction between the computational particles is "softened" at small separations, so that

close encounters are prevented letting the simulation run at a regular pace (Iannuzzi & Dolag, 2011). This softening length would be incorporated when REBOUND calculates the acceleration onto each particle. For a particle with index i this is given by:

$$\mathbf{a}_i = \sum_{j=0}^{N_{active}-1} \frac{Gm_j}{\left(r_{ij}^2 + b^2\right)^{3/2}} \hat{\mathbf{r}}_{ij}$$

where m_j is the mass of the particle j, $\mathbf{r}_{ji}$ is the relative distance between particles j and i, and b is the softening parameter. The N_{active} refers to the number of massive particles in the simulation, and particles with an index equal or larger than N_{active} are treated as test-particles (Rein & Liu, 2012b). The choice for parameter p in this simulations was:

$$b = 0.5 \cdot (\overline{r}_{ji})^{0.8}$$

in which $\overline{r}_{ji}$) is the average distance between the particles.

3.4 Put in orbit around MW potential

At this point we had a stable gravitational bound system in equilibrium as seen in first row of fig.9, so the next step was to perturb it with the gravitational forces from our galaxy. The MW potential function was a simplified spherical symmetric model, derived from a galactic potential of the python package GALPY (Bovy, 2015). The function would take the values from this simplified galactic grid and update the position of particles using the *additional forces* package in REBOUND. To accommodate this external force, a radial stripping radius had to be added, at which sources would become unbound from the system. This effect had to be incorporated to the NFW profile (eq.4) of the dwarf as an exponential since the 'stripping' would increase at larger radii:

$$\rho_{NFW}(r) = \rho_0 \left(\frac{r}{r_s}\right)^{-1} \left(1 + \frac{r}{r_s}\right)^{-2} \left(1 + \left(\frac{r}{r_t}\right)^4\right)^{-1} \tag{8}$$

where r_t would be the tidal stripping radius which we set to be 1500 pc, which is quite close in value to the scale length r_s and core model's r_c at 1000 pc. This is because the main focus was to see the result from tidal forces on satellites, so we wanted the effect from the gravitational perturbation to be as noticeable as possible while keeping it physically reasonable.

In addition, the simulated dwarf galaxy needed to be put into orbit around this MW potential which had been included. There are multiple dSph orbiting the centre of our galaxy, but we decided on Hercules

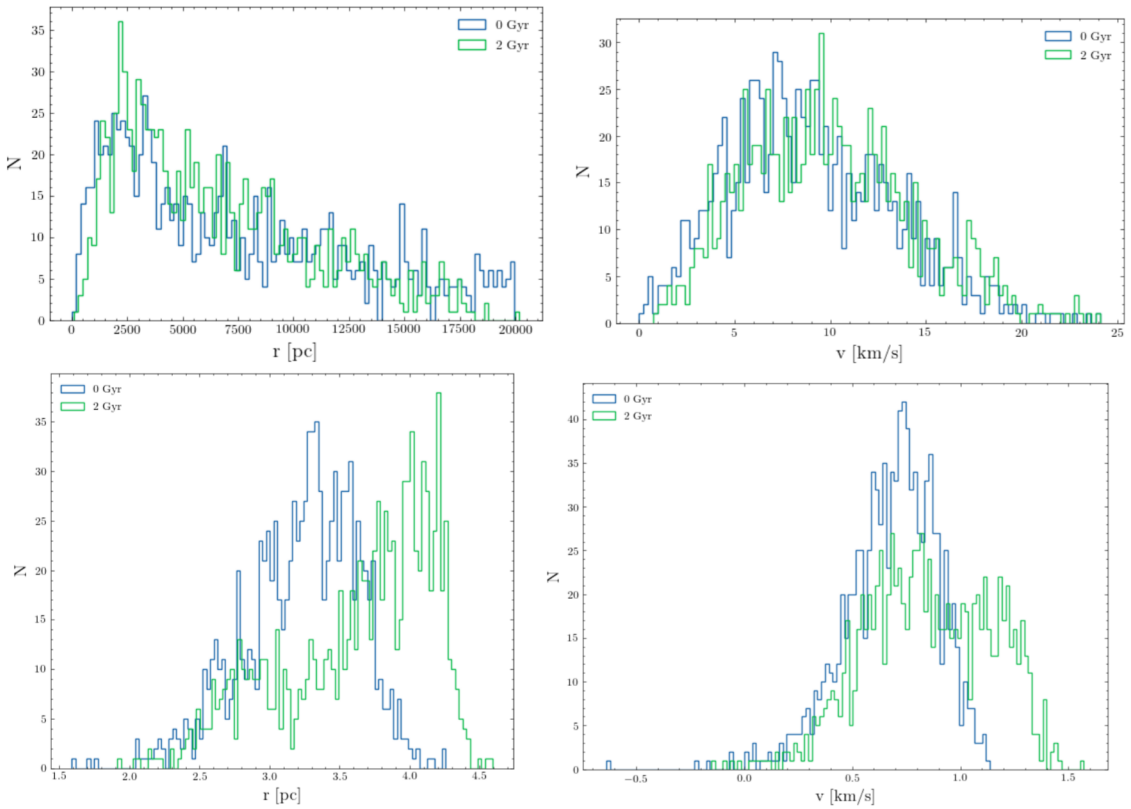

Figure 9: Graphs showing the initial and final distribution of the core NFW model after evolving the system using the REBOUND package. The simulation was of $N = 1000$ particles with a virial mass $M_{200} = 10^7\ M_\odot$, and the resulting softening length was of $b = 158$ pc. First row: no potential implemented to program. Second row: MW potential included in simulation as described in sec.3.4, and plots are in rest frame of the orbiting system.

(HerI) for the choice of trajectory, since signs of tidal disruption have been observed(Martin & Jin, 2010; Fritz et al., 2018), and given its large optical size, it is better resolved than other dwarfs (Putman et al., 2021). Also there is the fact that HerI is one of the few dSphs to show visible tidal disruption, considering its extremely elongated stellar distribution, along with kinematic substructures and velocity gradients (Li et al., 2018). The position and velocity data for HerI was taken from Li et al. (2021) which was based on the latest data release from Gaia (ED3) (Gaia Collaboration et al., 2021). The values given in Li et al. (2021) from which the position was infer were:

$$\theta = 51^\circ,\ \phi = 211^\circ,\ r_{GC} = 130 \text{ kpc}$$

being r_{GC} the Galactocentric distance. Hence, the initial cartesian coordinates introduced in the code were:

$$x = r_{GC} \sin\theta \cos\phi$$

$$y = r_{GC} \sin\theta \sin\phi$$

$$z = r_{GC} \cos\theta$$

Then, given the angles and velocity values:

$$v_r = 140 \text{ km/s},\ v_\theta = 130 \text{ km/s},\ v_\phi = -4 \text{ km/s}$$

so the initial velocity values for our system were:

$$v_x = v_r \sin\theta \cos\phi + v_\theta \cos\theta \cos\phi - v_\phi \sin\phi$$

$$v_y = v_r \sin\theta \sin\phi + v_\theta \cos\theta \sin\phi + v_\phi \cos\phi$$

$$v_z = v_r \cos\theta - v_\theta \sin\theta$$

The choice of values based on HerI trajectory were just the starting point, from which the simulated satellite started to orbit. Once this was in motion, the perturbation of our system was noticeable as visible in the second row of fig.9, in which we see a shift both on the spatial and velocity distribution of our system after 2 Gyr orbiting the MW potential.[1]

[1] All the programs and functions used during these project were written solely by me with advice from my supervisor, however the MW potential function was provided from the galpy package (Bovy, 2015).

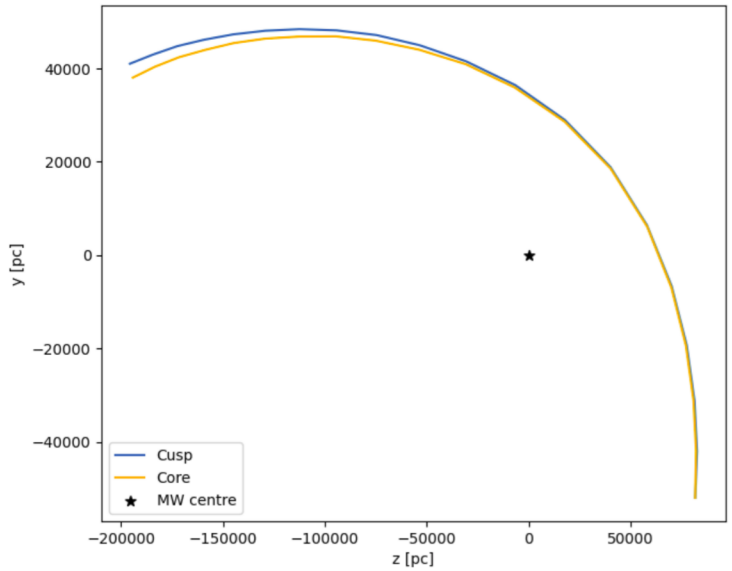

Figure 10: Trajectory of cusp and core NFW simulated dSph ($M_{200} = 10^8$) over 2 Gyr, based on HerI orbit around the MW.

Table 1: The overdensity parameter Δ, concentration parameter c_{200} and critical density of the universe ρ_{crit} were taken from Read et al. (2018).

N	Δ	h	c_{200}	$\rho_{crit}[M_\odot/kpc^3]$	$M_{200}[M_\odot]$	r_s [pc]	r_t [pc]
10^4	200	0.7	14	136.05	$3 \cdot 10^8$	1000	1500

4 Results

4.1 Results from evolution

Once the satellite was set in orbit, the aim was to check for possible disruptions as it was allowed to orbit the potential for a considerable amount of time (2 Gyr). Therefore, it was of main interest to check its morphology before and after the it would pass through the pericentre, as the most nearby position to the gravitational potential source, meaning the point were the gravitational pull is at its highest. In order to maximise the possible tidal effects, we started our simulations with a low total mass, hence of the order $M_T = 6 \cdot 10^7 M_\odot$. The variables introduced in the program for such mass were the ones stated in Table 1. These were inserted into eq.6from the previous chapter, using $n = 0$ for the cusp model, and $n = 1$ for the core model. When evolving independently each of the models, the core one reached the pericentre faster than the cusp one, with the core reaching it around the 600 Myr mark,

and the cusp at around 700 Myr. In addition, the core model also got closer to the potential by two units, compared to the cusp; hence, the core model seems to be more susceptible to the gravitational pull from the MW. The pericentre location from the gravitational source was ∼50 kpc in both models, which matches the observed value of 52 kpc for the HerI pericentre by *Gaia* (Li et al., 2021). The effect on their phase-space can be seen in fig.11 for the cusp profile, and fig.12 for the core profile. From the graphs, its visible the core profile gets more disrupted from its original form, than the cusp, especially noticeable after the pericentre passage, when some 'stretching' into spiral-like arms starts to happen. In the cusp model (fig.11 some 'stretching' is also noticeable after the passage through the pericentre, but much milder with only some faint pulling of its extremes after the pericentre, mostly retaining its original shape. These results seem to indicate that the cusp model would resist better against tidal disruptions than a core profile. Considering that a cuspy profile is more compact at its centre, it makes sense then that it would be harder to alter its morphology or pull tightly packed particles from its core. It's worth noting that the apparent disruption only seems visible when considering the velocity coordinates, which in the histograms would be from the third row down. Therefore, the spatial distribution doesn't seem to get as affected as the velocity one, so the kinematic signature of these profiles appears to be the key to differentiate between the two models.

To further dig into the apparent difference, the phase-space dispersion was plotted for similar time steps considered in the 2D histograms, seen in fig.13. Here the kinematic response to disruption of each model become even more noticeable, especially when looking at the end of the simulation (plots at the further right in fig.13). The evolution already points towards a more 'stream' behaviour in the core case shifting more of the overall morphology of the system than in the cusp one. Then, towards the end, the cusp model seems to have a 'breakage', in which the further away particles would escape the grasp of the system, with the leftover ones returning to the somewhat original shape. Thus, suggesting the central higher density region of the cusp profile would be left 'intact'.

4.2 Modifying density formulation

The truncated NFW profiles (eq.6) were mostly the ones used during the span of this project. However, it is true that despite their universal good fit of DM halos, it is not the only formulation being considered out there. Since we were aiming at maximising the possible differences between the profiles, a simpler

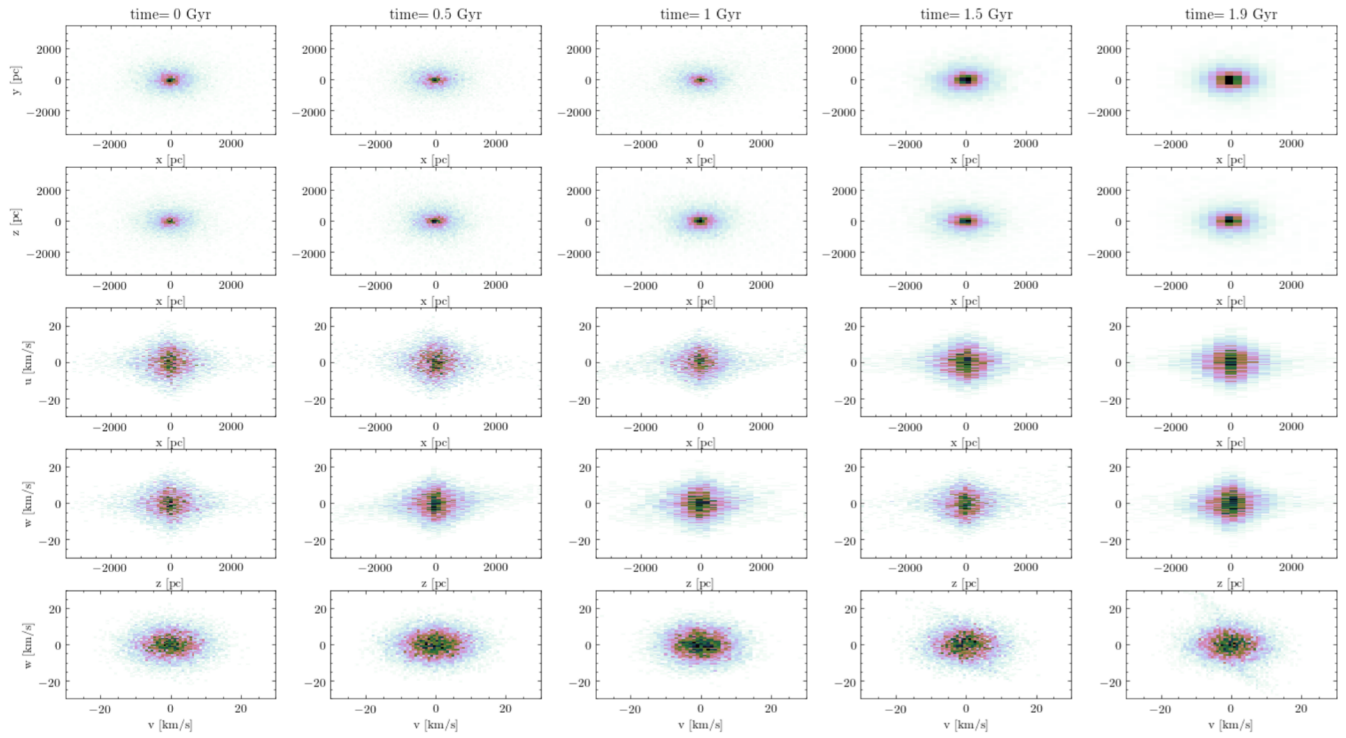

Figure 11: Cusp model 2D histograms in spatial (x, y, z) and velocity space (u, v, w) in the rest frame of the satellite, after being allowed to orbit for 2 Gyr in the simulation. The pericentre passage happens at 700 Myr, so between the second and third column starting from the left.

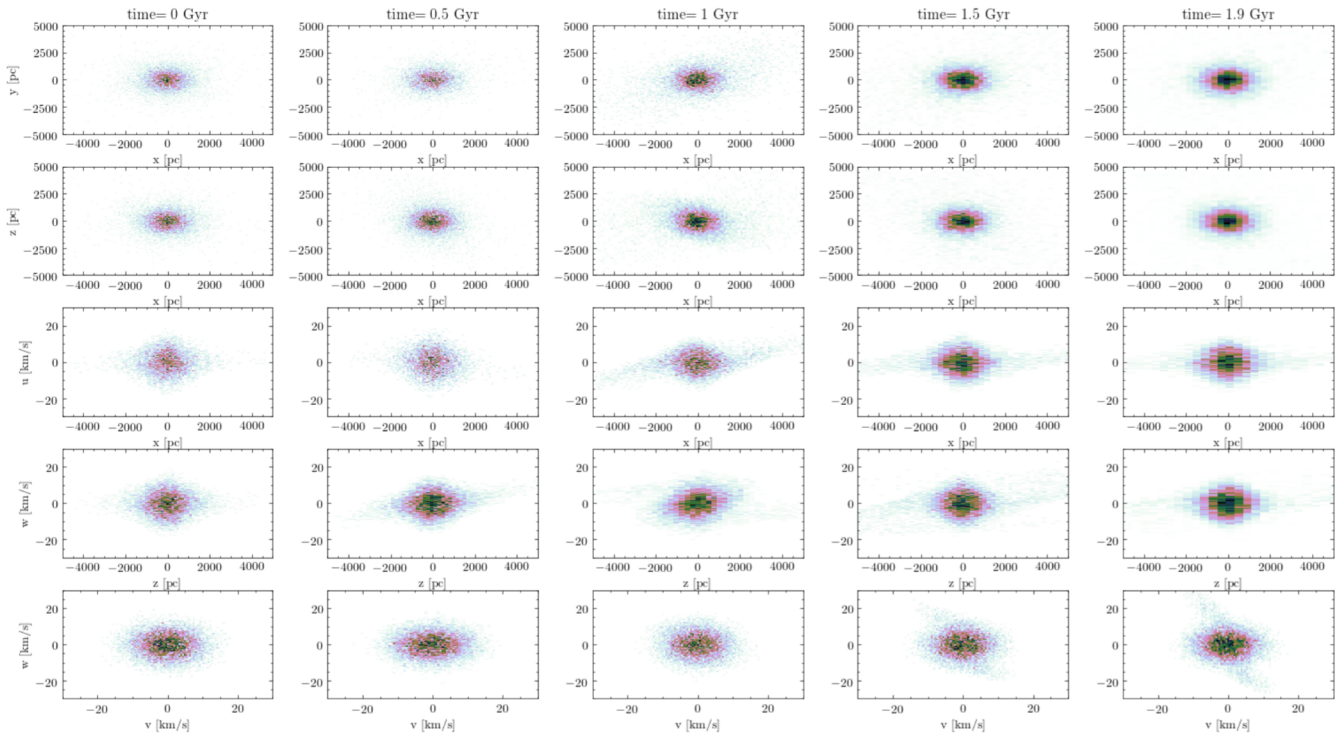

Figure 12: Core model 2D histograms in spatial (x, y, z) and velocity space (u, v, w) in the rest frame of the satellite, after being allowed to orbit for 2 Gyr in the simulation.The pericentre passage happens at 600 Myr, so between the second and third column starting from the left.

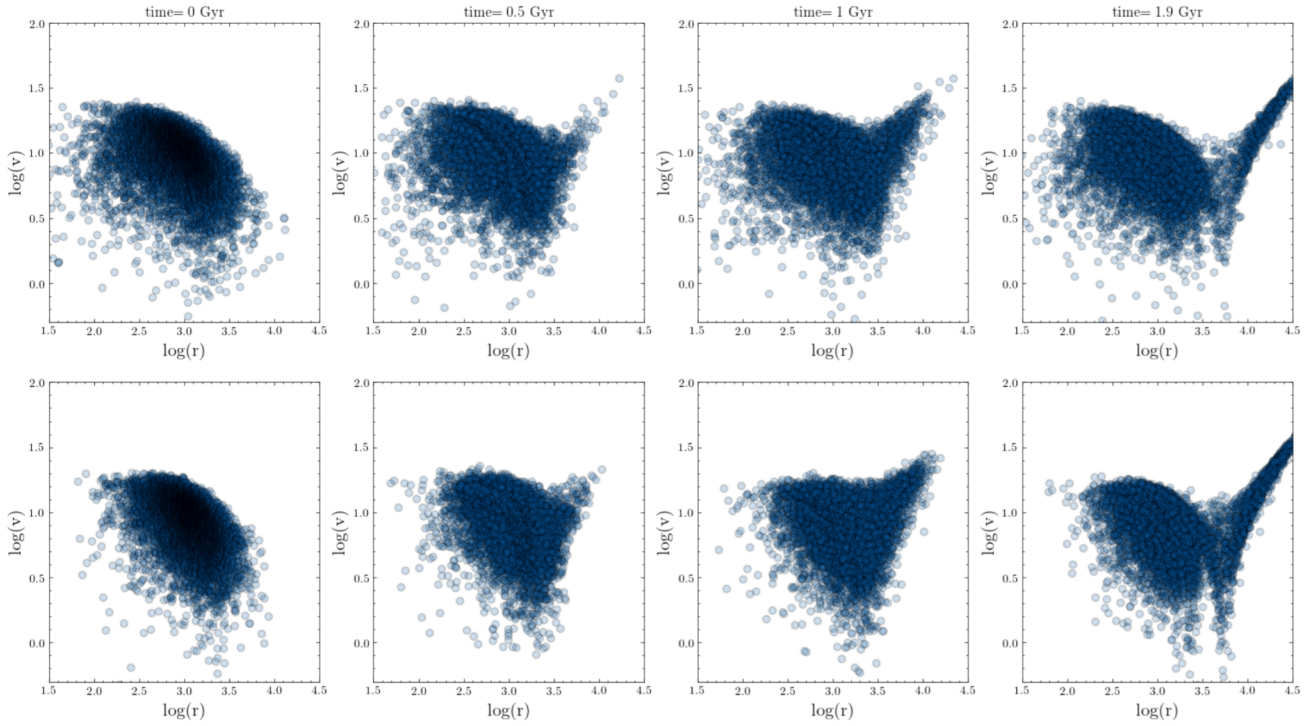

Figure 13: Radius versus velocity dispersion evolution for a total mass of $10^7 M_\odot$ using the profile formulation stated in eq. 6 in Chapter 3. **Top row**: Cusp profile. **Bottom row**: Core profile. Both obtained using variables from table 1

Table 2: The central densities chosen for each profile in order to obtain a certain total mass for the system.

	$10^7 M_\odot$	$10^8 M_\odot$	$10^9 M_\odot$
ρ_0 (Cusp) [$M_\odot/pc^3$]	0.0024	0.024	0.24
ρ_0 (Core) [$M_\odot/pc^3$]	0.0052	0.052	0.52

formulation was tested at the end of the project. The aim was to be able to vary the mass of the system in a simpler way, without having to modify complex parameters as the overdensity of the core (Δ) or the concentration parameter (c_{200}). Therefore, we kept the original NFW profile for the cusp model (eq.8), since it fits well such steep model. The value of ρ_0 this time wasn't obtained from other variables, instead it was decided by a numerical approach, in which ρ_0 would be tuned so that the total mass of the system (eq.7, would be the one desired. The simplification of the core profile was more drastic, dropping the function f^n that provided a shallower profile when implemented in the cuspy formula, and instead just raising the power in the denominator to flatten out the function at low radii, unlike the parabolic increase in density the cusp suffers at the origin ($r = 0$). The ρ_0 was also estimated numerically in order to obtain the same order of total mass as the cusp model. Hence, their respective density expressions, including the radial stripping term, were:

$$\rho_{cusp}(r) = \rho_0 \left(\frac{r}{r_s}\right)^{-1} \left(1 + \frac{r}{r_s}\right)^{-2} \left(1 + \frac{r}{r_t}\right)^{-4}$$

$$\rho_{core}(r) = \rho_0 \left(1 + \frac{r}{r_s}\right)^{-3} \left(1 + \frac{r}{r_t}\right)^{-4}$$

where once again we used the scale length $r_s = 1000$ pc, the tidal radius $r_t = 1500$ pc, and the central density ρ_0 was varied for different orders of total mass of the system and respective model. The values selected in the end for the central density are shown in table2, and as expected the higher the mass of the system, the higher the density ρ_0. Also, we see how the core model needs to be about double the value of the cusp to reach the same order of total mass. Considering the higher power in the denominator of ρ_{core} compared to ρ_{cusp}, the density will drop more rapidly in the core model and since the mass is estimated from the accumulated mass function (eq.2) the faster decrease in $\rho(r)$ requires a higher starting value for the core model.

In the previous subsection, with the NFW truncated profiles, we were considering a system with a

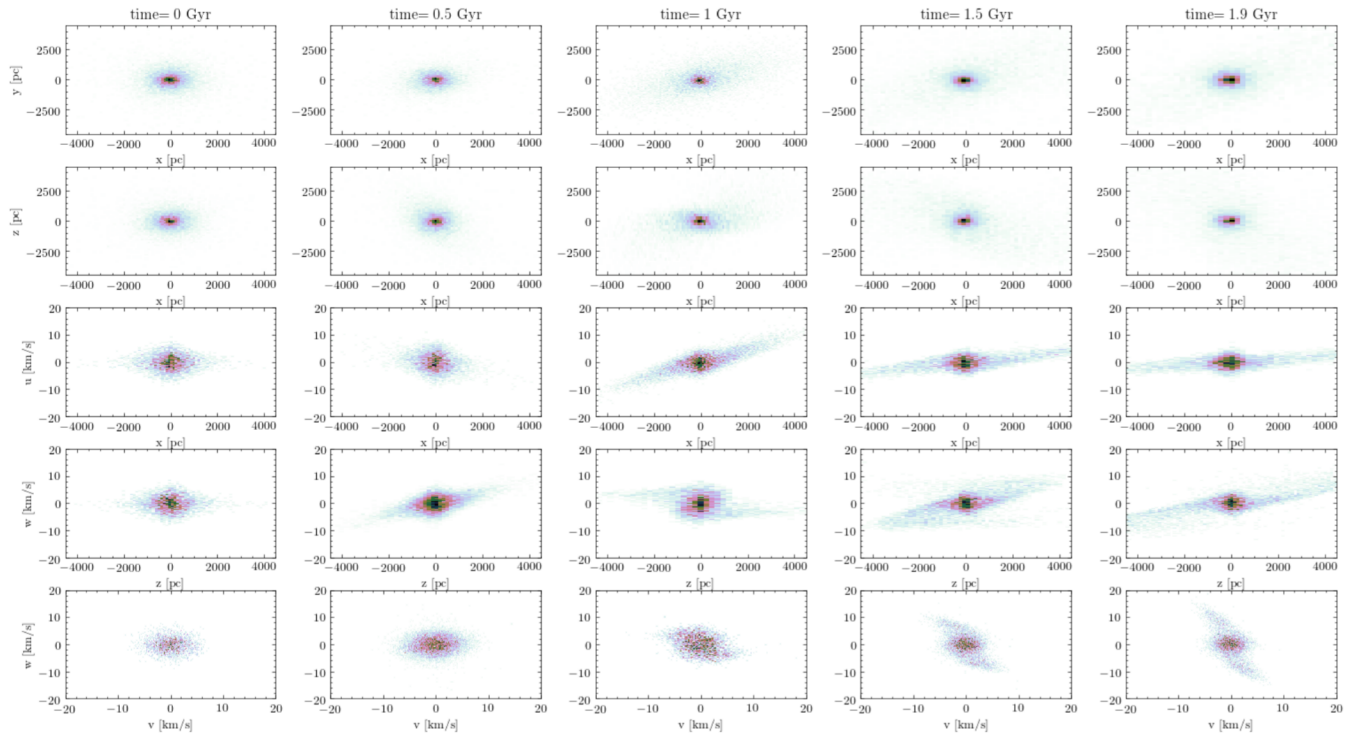

Figure 14: Cusp model 2D histograms in spatial (x, y, z) and velocity space (u, v, w) in the rest frame of the satellite, using the simpler formulation described in section 4.2 for a total mass of $10^7 M_\odot$.The pericentre passage happens at 700 Myr, so between the second and third column starting from the left.

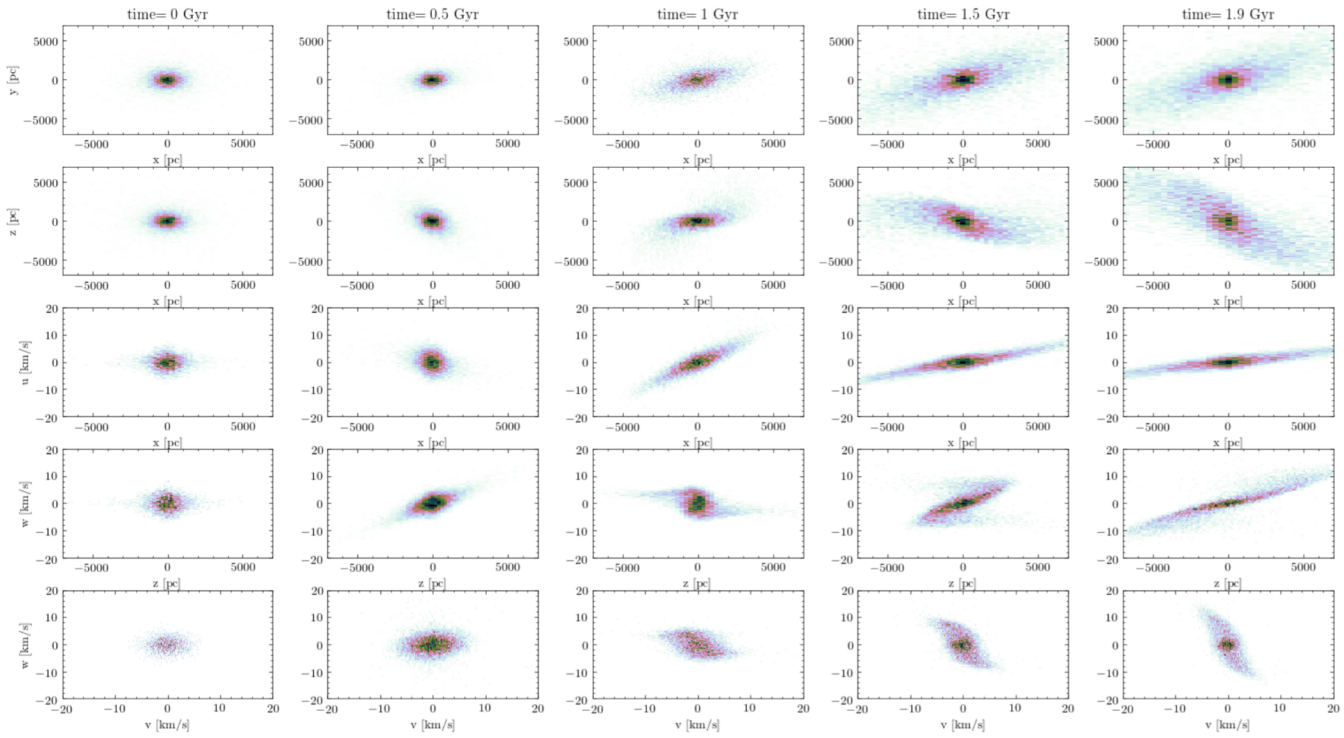

Figure 15: Core model 2D histograms in spatial (x, y, z) and velocity space (u, v, w) in the rest frame of the satellite, using the simpler formulation described in section 4.2 for a total mass of $10^7 M_\odot$.The pericentre passage happens at 600 Myr, so between the second and third column starting from the left.

total mass of the order of $10^7 M_\odot$. Therefore, we can compare the previous results with the evolution shown in figures 14 and 15, which are from a system with the same order of total mass but using the simpler formulation. Clearly this new formulation is more susceptible to tidal disruptions, both for the cusp and core case, with the histograms showing a 'stretching' of the system, and even 'spiraling' behaviour, after the pericentre passage. Something interesting in fig.15 (core model), is how this time we do observe a deformation of the system even when looking only at the spatial coordinates (first two rows). This was not happening with the NFW truncated core profile, and furthermore, the 'stretching' at the edges of the system is unmistakable. In fact, the 'stretching' after the pericentre, meaning from the third column onwards, turns into what could be called 'arms', that end up spiraling (s-shaped) as if the system was rotating on itself. These 'arms' formation, is also visible in the cusp model (fig.14, however is less dramatic and the stretching of the original morphology isn't as extreme towards the end of the simulation. In addition, the cusp model doesn't show a deformation when looking at the spatial coordinates alone (first two rows), suggesting once again that the cusp spatial morphology is more resilient against deformation.

The higher susceptibility of this new density formulation, was evident when looking at the phase-space dispersion. The kinematic signatures of each model were more discernible, following similar trends observed with the previous formulation. The phase-space evolution of the system for each of the total masses considered in table2, can be seen in figures 16, 17 and 18. The first figure 16, has the same total mass ($10^7 M_\odot$) used for the plot with the previous formulation in figure 13. When looking at this plot (fig.16), it becomes more obvious how the core model showed disruption in the spatial coordinates as well as in the velocity ones (fig.15). By the end of the simulation the core model in fig.16 (second row, far right), has turned into a ribbon-like structure, resembling a stream, which is quite a change from its initial more compact structure (second row, far left). On the other hand, the cusp model (top row), also experiences a stronger deformation of its original morphology, but the disruption is more localised, just affecting particles at the edge of the system. Reason why in its histogram, the spatial coordinates did not show a disruption as it happened in the core model. At the end of the simulation (top row, far right), the original morphology of the cusp model is still present with an additional peak-like substructure from the tidal pull. This peak-like structure appears still when we incremented the mass by one order, as seen in fig.17. Here, both profiles show such peak at the end of the simulation, with the core model retaining

more of its original shape this time. Even if both profiles show a similar substructure from the tidal pull, there is still a clear difference on the final result of each model. The core model might not have gotten as stretched as in the previous case with a lower mass system, yet more of its overall structure gets modified in shape following the tidal pull, than in the cusp case. Indeed more particles get pulled from the core profile under the gravitational attraction of the MW, than in the cusp, which becomes even more apparent in fig.18 with the system highest in mass. The results for the $10^8 M_\odot$ system, resemble the ones obtained with the previous density formulation, where the cuspy profile once again shows a 'break off' from the peak-like substructure, retaining most of its particles and original morphology; meanwhile, the core system gets more distorted suffering a further re-structuring of its overall morphology. With the increment of mass up to $10^9 M_\odot$, the systems are much sturdier against disruption given the stronger gravitational binding energy. Consequently, only a few particles seem to suffer the pull from each of the models at the end of the simulation, with the core having more particles drifting off. Thus, as mentioned before, it is still visible that the core model suffers a greater distortion.

Altogether, both density formulations suggest that the core model leans towards a stream-like behaviour, modifying its overall morphology, while the cusp model tends to retain its original form within the central region, while the 'stretching' only affects a smaller number of particles located closer to the potential. Concluding that a cusp and a core profile have distinct kinematic responses to tidal disruptions from the gravitational potential they orbit.

4.3 Median variability

To measure the variability and range of the data through the evolution of the system, the median of the spatial location and velocity were checked. Considering the previous plots, were we could see the disruption from the tidal forces affected especially the outliers; the median was a better choice than the mean for this analysis, since the median is less affected by the behaviour of outliers which might skew the average. When doing so, it was of special interest to look at the velocity, due to the more apparent disruption in velocity space observed in previous plots. As expected, the median of velocity varied more throughout the evolution of the system, than that of the spatial location. In fig.19 this variability can be observed, where both the median velocities for the $10^7 M_\odot$ and $10^8 M_\odot$ systems are plotted. We focused on these two cases since their dispersion plots (fig.16, fig.17) showed more prominent disruptions from

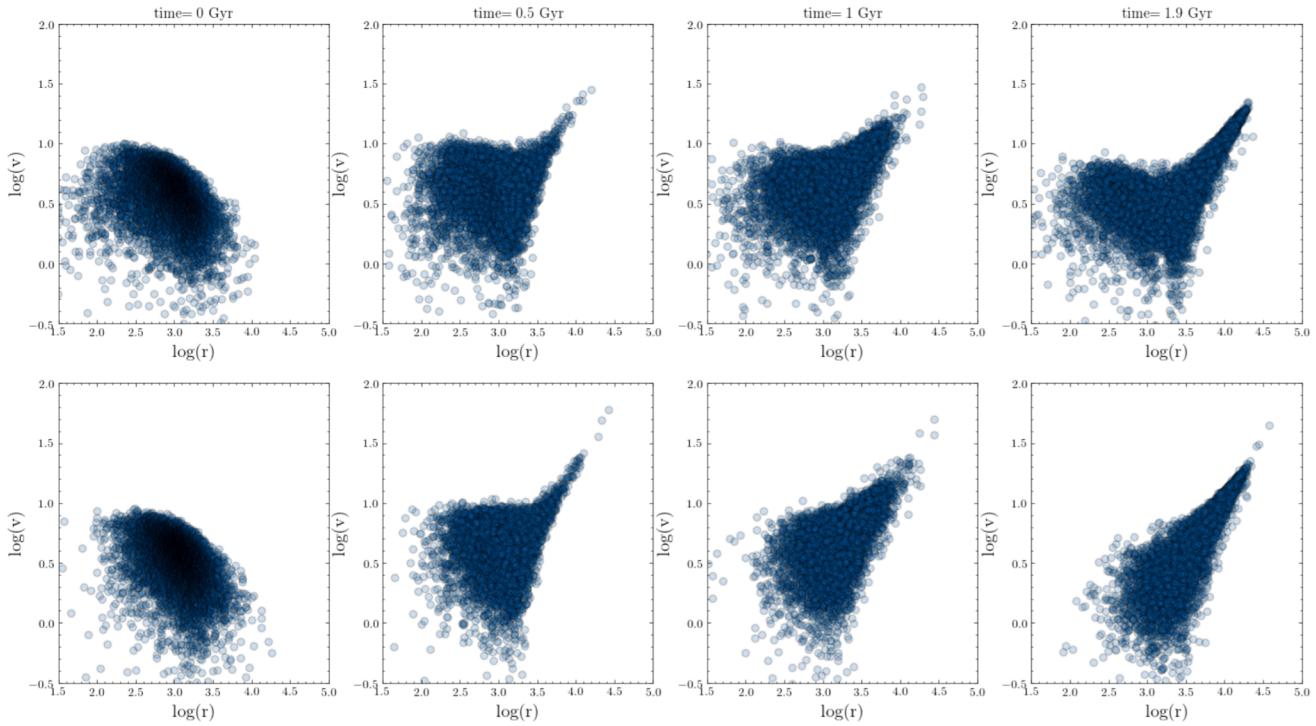

Figure 16: Radius versus velocity dispersion evolution for a system with a total mass of $10^7 M_\odot$. **Top row**: Cusp profile. **Bottom row**: Core profile.

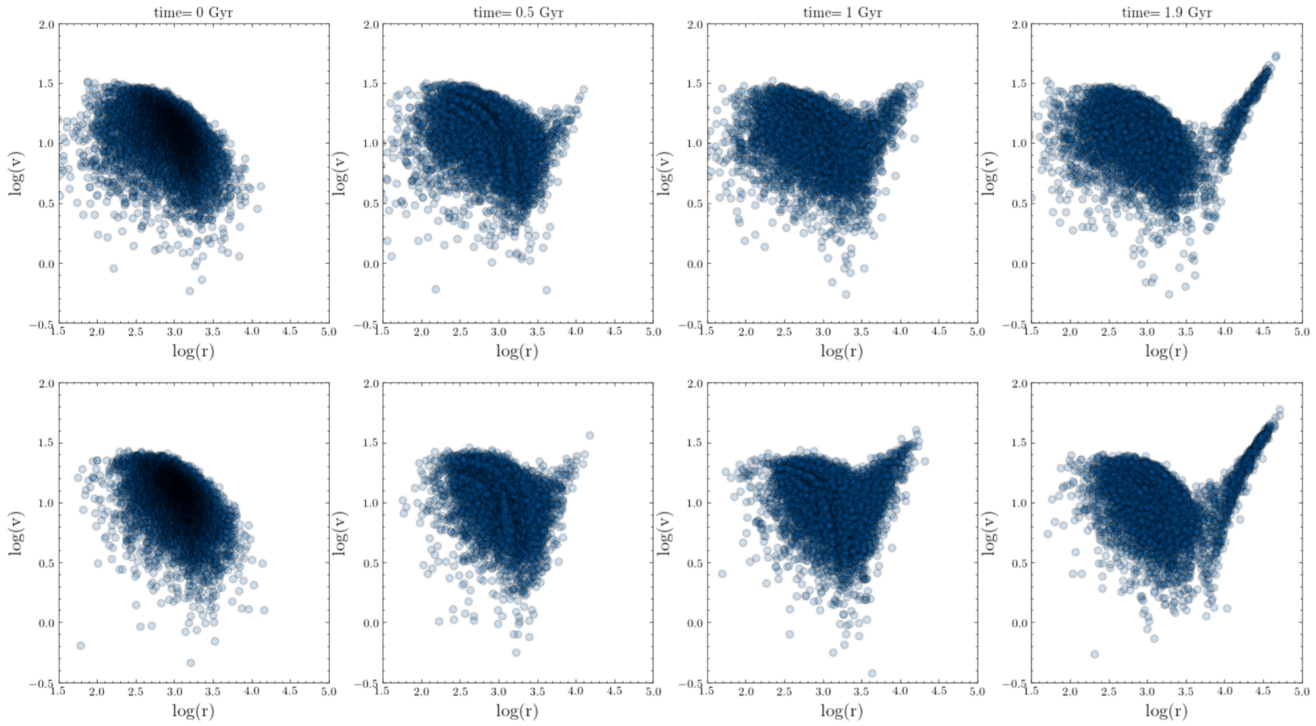

Figure 17: Radius versus velocity dispersion evolution for a system with a total mass of $10^8 M_\odot$. **Top row**: Cusp profile. **Bottom row**: Core profile.

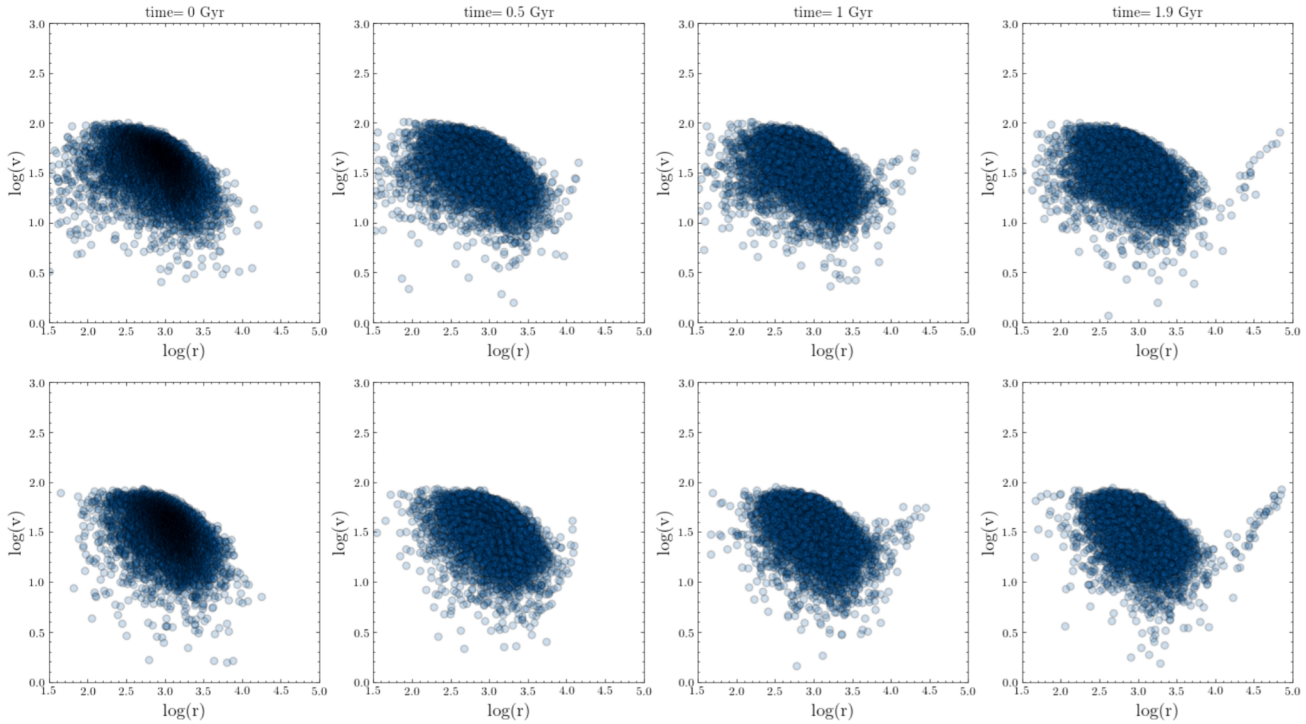

Figure 18: Radius versus velocity dispersion evolution for a system with a total mass of $10^9 M_\odot$. **Top row**: Cusp profile. **Bottom row**: Core profile.

the tidal forces. In both of these graphs of the median of the velocity, a peak on their velocity value appears after their pericentre passage, going down again afterwards. Also, the cusp model reaches higher median velocity than the core model does.

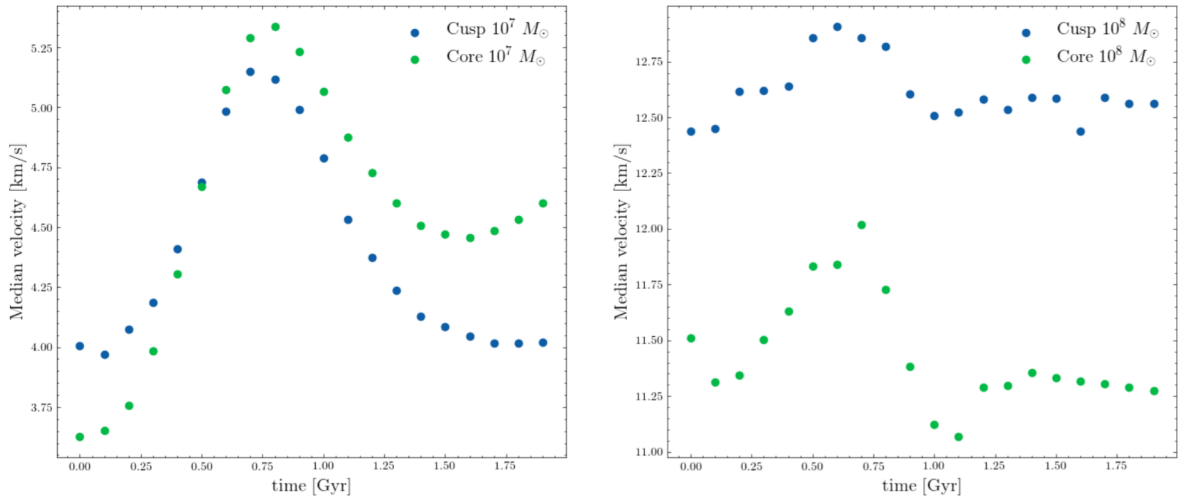

Figure 19: Median of velocity for the simpler formulation, focusing on the simulations in which the tidal disruption to their phase-space morphology was more noticeable. **Left**: $10^7 M_\odot$. **Right**: $10^8 M_\odot$.

5 Discussion

In the previous chapter, we presented the different kinematic responses cusp and core profiles exhibited when being exposed to tidal forces from a gravitational potential for a 2 Gyr period. It was stated before how the core profile got closer to the potential, and reached its pericentre faster in its orbit than the cusp one did. This already seemed to indicate the stronger pull a shallower density profile would experience in the presence of tidal forces, compared to a steep one. Such statement was confirmed by the kinematic behaviour of the simulated satellites. The gravitational binding energy of the system its proportional to its mass, hence the lowest the total mass, the easier for the tidal forces to strip particles from the system. Still, even at the lowest mass considered ($10^7 M_\odot$), the cusp model, with a steeper density profile, kept retaining most of its original morphology. The disruption was evident, seen in the peak-like substructure, but the overall structure did not get modified drastically. On the other hand, the shallower density profile, meaning the core model, turned into a steam-like structure, loosing its initial shape completely. The changes were also visible in the 2D histograms, in which the 'arms' developed at the edges of the structure ended up 'spiraling' (s-shaped) hinting towards possible self-rotation of the system. There has been suggestions of self-rotating dwarf satellites, yet as said previously, most dSphs do not seem to show a really noticeable rotation of that kind. Although, it must be considered that the apparent 'spiraling' (s-shapes) does not appear at higher masses (histograms for higher masses can be found in the appendix). Therefore, the lack of data for prominent self-rotation could either favour

cuspy profiles over core ones, or just be due to satellites having a higher total mass. Also, if the density distribution was more similar to the truncated NFW than the simpler formulation, perhaps lower masses could also not exhibit such s-shapes.

When considering the median velocity plots (fig.19), it is clear there is a peak in both models after the pericentre passage, which happens at around 600 Myr for the core and 700 Myr for the cusp. After this peak, the median velocity returns to its value before such disruption. It is also noticeable that the cusp profile reaches a higher median velocity than the core one. Considering the high density of particles at the central core of the cusp model, it would allow for high velocities to be reached, which would rapidly decrease with the steep slope of the density as the radii increases. Still, the variability of the median velocity is similar in both models, although it seems more prominent in the core model when looking at the higher mass system. A hypothesis for this slightly different behaviour for each model could be that the cusp model stabilises back itself by allowing the disrupted 'tail', meaning particles at the edge being pulled by tidal forces forming a peak-like substructure, to break off from the main structure. Meanwhile, the core model would adopt more of a stellar stream behaviour allowing such 'tail' to be part of its main structure, and just readjusting its shallow profile to accommodate the possible spatial modification.

5.1 Relation to baryonic phenomena & DM nature

At the start of this thesis it was stated that aside from data errors, which nowadays with the constant increase of accuracy in the kinematic data seems most unlikely, there were two other solutions for the cusp-core debate: baryonic interactions or changes in our understanding of the nature of DM. In the baryonic approach, the interesting argument was the possibility of cusp-core transformations. In our results, the cusp profile appears to have a 'break off' from the outliers that get tidally disrupted, while its central core would remain mostly intact. As mentioned before, this resilience makes it a better candidate for satellites to be able to survive until today. In addition, the loss of the outliers, could aid in the transformation process of a cusp into a core, since it would be getting rid of the particles at larger radii. Such effect added to other feedback processes as supernovae explosion, would over time grind the steep cusp profile into a constant density core one. Therefore, tidal disruption could be an asset in cusp-core transformations. On the other hand, the kinematic response from the core model, going into a stream-like behaviour, matches the theories that favour core profiles to solve the missing satellites

problem. A stellar stream is understood to be the middle step in the accretion of a smaller structure by a bigger host, in which a globular cluster or dwarf galaxy would have been stretched out and torn apart by the tidal forces of the host. Therefore, the core kinematic signature seems in tune with such scenario, the issue would be to determine if the cusp-core transformation would happen at a fitting time so that the system could survive, while still allowing many of them to undergo accretion before our current time.

Considering the possible cusp-core transformations that the tidal forces could enhance, the Warm DM model would be the least favourable, since it would delay the formation of substructures, which would put a tight schedule on the satellites evolution. Still, considering its delay at forming substructures would result in lower densities, favouring constant density cores. However, both with the Warm and Self-Interacting DM, the fact that they would produce lower density cores, might not be beneficial when considering the effects of processes as violent relaxation, which would jeopardise the survive of less dense systems. Hence, the Fuzzy DM seems interesting, as it would still retain much of the CDM features, while also predicting core profiles. However, it could also be that all satellites have core profiles, just with really large masses DM, which are harder to disrupt as seen in our results; therefore, still allowing all to be a possibility.

5.2 Observational data and future applications

Observations of the kinematics of these satellites would be the key to constraining the DM natures, yet it still remains a challenge to estimate the mass of these faint dwarf galaxies given the significant foreground contamination. The satellite used for the trajectory, HerI, has been estimated to have a low mass around $10^6 M_\odot$ (Sand et al., 2009). Therefore, taking in account our results, it comes as no surprise that tidal disturbances have been observed in its spatial distribution, and the main hypothesis is that its embedded in a larger stream of stars (Johnston et al., 1996; Ibata et al., 2019). Thus, our data could point towards a core profile, yet it should be noted that at low masses the cusp profile also suffered a noticeable disruption. Still, given it shows signs of spatial disturbance, and the 2D histograms of the cusp model did not show disruption in the spatial coordinates; the core profile seems most likely.

The next step would be to implement the star motion from the latest accurate surveys in these simulations to test how much of the morphology would be affected by the tidal disruption the DM halos experienced. Furthermore, the distinct kinematic signatures obtained in our study could be used as tools

if they were to be implemented into data machine learning. This way, surveys of kinematic data could be analysed and categorised based on their kinematic signature, providing a powerful tool to tackle the cusp-core debate, and hence, the nature of DM and formation of structures.

6 Conclusion

In this project we set out to study the kinematic response a cusp and a core density profile would have to tidal disruptions from a gravitational potential. An N-body simulation was built, in which each profile could be given as an input, and a simulated satellite of a chosen mass would be put into an orbit similar to that of HerI for a 2 Gyr period. The results showed a distinct kinematic signature for each of the models: the cusp model only was disrupted in velocity space, and the disruption was limited to the outliers keeping mostly its original morphology throughout and 'breaking off' from the tidal disrupted particles. The core model was disrupted both in velocity and also in spatially, if low enough total masses were considered. The overall morphology of the core model would shift into a stream-like structure, although this would be partly suppressed if the total mass would be large enough ($10^9 M_\odot$). Thus, proving shallow profiles are more susceptible. The core profile results of turning into a stream, fit the observational data from the HerI satellite from which the trajectory parameters were taken. Yet, their relevance to constrain DM nature would need to take in account more of the kinematic observational data to better determine the mass range the dwarf galaxies would fall in.

The next step for this study of DM halos profiles, would be to implement the tracer population in order to analyse how or if these tidal disruptions would significantly affect the stellar distribution, which is the one we can directly get kinematic data from. Finally, the idea would be to implement these results into data machine learning, so that the observational data would be directly categorised depending on its kinematic signature, helping in the quest for DM nature candidates.

References

Abell, G. O. 1959, Leaflet of the Astronomical Society of the Pacific, 8, 121

Alarcón Jara, A. G., Fellhauer, M., Matus Carrillo, D. R., et al. 2018, , 473, 5015

Alcock, C., Allsman, R. A., Alves, D. R., et al. 2000, , 542, 281

Amaré, J., Cebrián, S., Cintas, D., et al. 2021, , 103, 102005

Anderhalden, D., Schneider, A., Macciò, A. V., Diemand, J., & Bertone, G. 2013, , 2013, 014

Arcadi, G., Dutra, M., Ghosh, P., et al. 2018, European Physical Journal C, 78, 203

Arraki, K. S., Klypin, A., More, S., & Trujillo-Gomez, S. 2014, , 438, 1466

Arun, K., Gudennavar, S. B., & Sivaram, C. 2017, Advances in Space Research, 60, 166

Battaglia, G., Taibi, S., Thomas, G. F., & Fritz, T. K. 2022, , 657, A54

Bernabei, R., Belli, P., Bussolotti, A., et al. 2018, Universe, 4, 116

Bertone, G., & Hooper, D. 2018, Reviews of Modern Physics, 90, 045002

Bertone, G., Hooper, D., & Silk, J. 2005, , 405, 279

Blumenthal, G. R., Faber, S. M., Primack, J. R., & Rees, M. J. 1984, , 311, 517

Bode, P., Ostriker, J. P., & Turok, N. 2001, , 556, 93

Bovy, J. 2015, , 216, 29

Boyarsky, A., Drewes, M., Lasserre, T., Mertens, S., & Ruchayskiy, O. 2019, Progress in Particle and Nuclear Physics, 104, 1

Bullock, J. S., & Boylan-Kolchin, M. 2017, , 55, 343

Carlson, E. D., Machacek, M. E., & Hall, L. J. 1992, , 398, 43

Contenta, F., Balbinot, E., Petts, J. A., et al. 2018, , 476, 3124

Dalcanton, J. J., & Hogan, C. J. 2001, , 561, 35

Davis, M., Efstathiou, G., Frenk, C. S., & White, S. D. M. 1985, , 292, 371

de Blok, W. J. G. 2010, Advances in Astronomy, 2010, 789293

de Swart, J. G., Bertone, G., & van Dongen, J. 2017, Nature Astronomy, 1, 0059

Del Popolo, A. 2009, , 698, 2093

Del Popolo, A., & Le Delliou, M. 2021, Galaxies, 9, 123

Drukier, A. K., Freese, K., & Spergel, D. N. 1986, , 33, 3495

Einasto, J., Kaasik, A., & Saar, E. 1974, , 250, 309

Elbert, O. D., Bullock, J. S., Garrison-Kimmel, S., et al. 2015, , 453, 29

Elson, R. 2018, A Responsability to Awe (Carcanet Classics)

Errani, R., Navarro, J. F., Ibata, R., & Peñarrubia, J. 2022, , 511, 6001

Feng, J. L. 2010, , 48, 495

Flores, R. A., & Primack, J. R. 1994, , 427, L1

Freese, K. 2017, International Journal of Modern Physics D, 26, 1730012

Freese, K., Fields, B., & Graff, D. 2000, arXiv e-prints, astro

Frenk, C. S., & White, S. D. M. 2012, Annalen der Physik, 524, 507

Fritz, T. K., Battaglia, G., Pawlowski, M. S., et al. 2018, , 619, A103

Gaia Collaboration, Brown, A. G. A., Vallenari, A., et al. 2021, , 649, A1

Gao, L., Navarro, J. F., Frenk, C. S., et al. 2012, , 425, 2169

González-Samaniego, A., Bullock, J. S., Boylan-Kolchin, M., et al. 2017, , 472, 4786

Hammer, F., Yang, Y., Arenou, F., et al. 2018, , 860, 76

Hu, W., Barkana, R., & Gruzinov, A. 2000, , 85, 1158

Iannuzzi, F., & Dolag, K. 2011, , 417, 2846

Ibata, R. A., Bellazzini, M., Malhan, K., Martin, N., & Bianchini, P. 2019, Nature Astronomy, 3, 667

Johnston, K. V., Hernquist, L., & Bolte, M. 1996, , 465, 278

Klasen, M., Pohl, M., & Sigl, G. 2015, Progress in Particle and Nuclear Physics, 85, 1

Klypin, A., Kravtsov, A. V., Valenzuela, O., & Prada, F. 1999, , 522, 82

Kuhlen, M., Vogelsberger, M., & Angulo, R. 2012, Physics of the Dark Universe, 1, 50

Laporte, C. F. P., & Penarrubia, J. 2015, , 449, L90

Li, H., Hammer, F., Babusiaux, C., et al. 2021, , 916, 8

Li, T. S., Simon, J. D., Kuehn, K., et al. 2018, , 866, 22

Martin, N. F., & Jin, S. 2010, The Astrophysical Journal, 721, 1333

McMillan, S. 2022, Computational Physics II Drexel University

Miholics, M., Webb, J. J., & Sills, A. 2014, , 445, 2872

Moore, B., Ghigna, S., Governato, F., et al. 1999, , 524, L19

Muñoz, C. 2004, International Journal of Modern Physics A, 19, 3093

Navarro, J. F., Eke, V. R., & Frenk, C. S. 1996a, , 283, L72

Navarro, J. F., Frenk, C. S., & White, S. D. M. 1996b, , 462, 563

Navarro, J. F., Ludlow, A., Springel, V., et al. 2010, , 402, 21

Okabe, N., Smith, G. P., Umetsu, K., Takada, M., & Futamase, T. 2013, , 769, L35

Ostriker, J. P., Peebles, P. J. E., & Yahil, A. 1974, , 193, L1

Parmentier, G. 2009, Reviews in Modern Astronomy, 21, 183

Pawlowski, M. S. 2021, Galaxies, 9, 66

Peebles, P. J. E. 1982, , 263, L1

Petts, J. A., Read, J. I., & Gualandris, A. 2016, , 463, 858

Pils, K., & Rindler-Daller, T. 2022, arXiv e-prints, arXiv:2202.12779

Plummer, H. C. 1911, , 71, 460

Putman, M. E., Zheng, Y., Price-Whelan, A. M., et al. 2021, , 913, 53

Read, J. I., Agertz, O., & Collins, M. L. M. 2016, , 459, 2573

Read, J. I., & Gilmore, G. 2005, , 356, 107

Read, J. I., Walker, M. G., & Steger, P. 2018, , 481, 860

Rein, H., & Liu, S. F. 2012a, , 537, A128

—. 2012b, , 537, A128

Rocha, M., Peter, A. H. G., Bullock, J. S., et al. 2013, , 430, 81

Rubin, V. C., & Ford, W. Kent, J. 1970, , 159, 379

Sand, D. J., Olszewski, E. W., Willman, B., et al. 2009, , 704, 898

Schneider, A., Trujillo-Gomez, S., Papastergis, E., Reed, D. S., & Lake, G. 2017, , 470, 1542

Shane, C. D., & Wirtanen, C. A. 1954, , 59, 285

Shukirgaliyev, B., Otebay, A., Sobolenko, M., et al. 2021, , 654, A53

Spergel, D. N., & Steinhardt, P. J. 2000, , 84, 3760

Taoso, M., Bertone, G., & Masiero, A. 2008, , 2008, 022

Tollerud, E. J., Bullock, J. S., Strigari, L. E., & Willman, B. 2008, , 688, 277

Trimble, V. 1987, , 25, 425

Valenzuela, O., Rhee, G., Klypin, A., et al. 2007, , 657, 773

Weinberg, M. 2020, Notes on generating initial conditions using Eddington's inversion

Wheeler, C., Pace, A. B., Bullock, J. S., et al. 2017, , 465, 2420

White, S. D. M., Frenk, C. S., & Davis, M. 1983, , 274, L1

Zolotov, A., Brooks, A. M., Willman, B., et al. 2012, , 761, 71

Zwicky, F. 1937, , 86, 217

7 Appendix

In the appendix some additional graphs regarding the results are presented, which did not seem essential to explanation exposed in the thesis, but that could still be of interest. At the end there is also an inspiring poem regarding the search of dark matter by a past astrophysicist (Elson, 2018), which I found quite fitting to the end of this project.

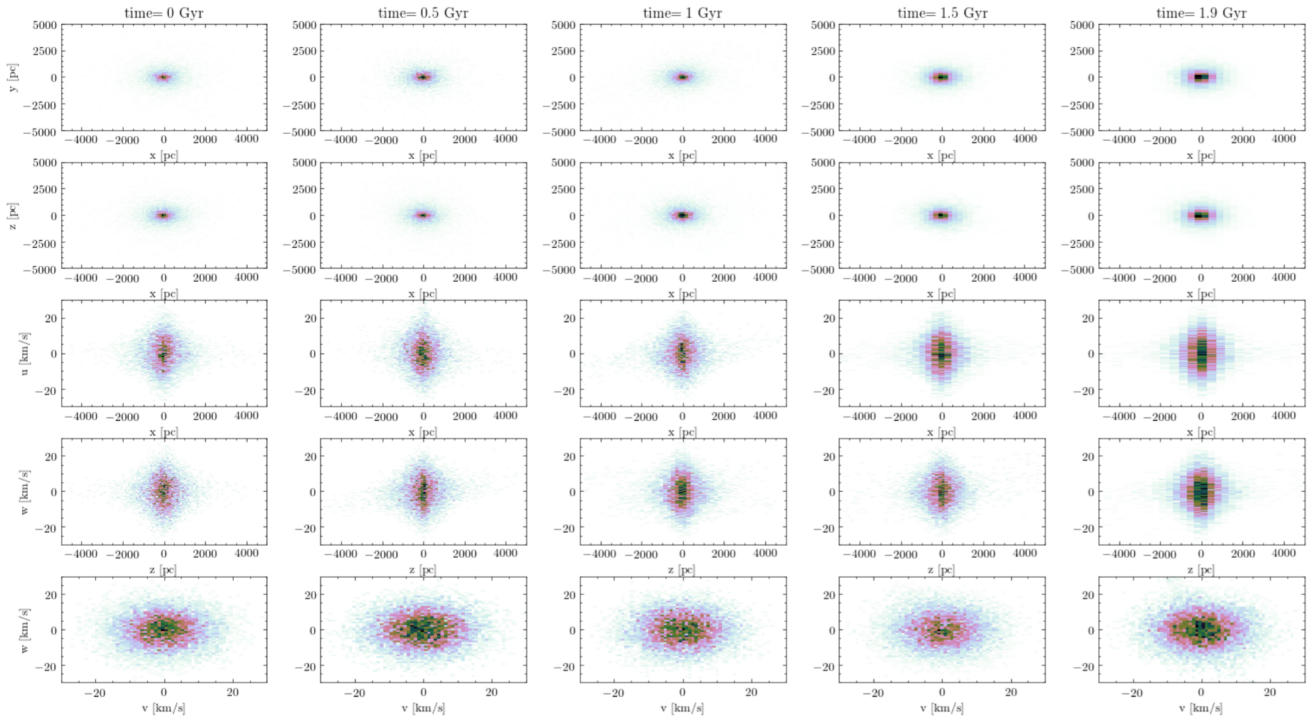

Figure 20: Cusp model 2D histograms in spatial (x, y, z) and velocity space (u, v, w) in the rest frame of the satellite, using the simpler formulation described in section 4.2 for a total mass of $10^8 M_\odot$.The pericentre passage happens at 700 Myr, so between the second and third column starting from the left.

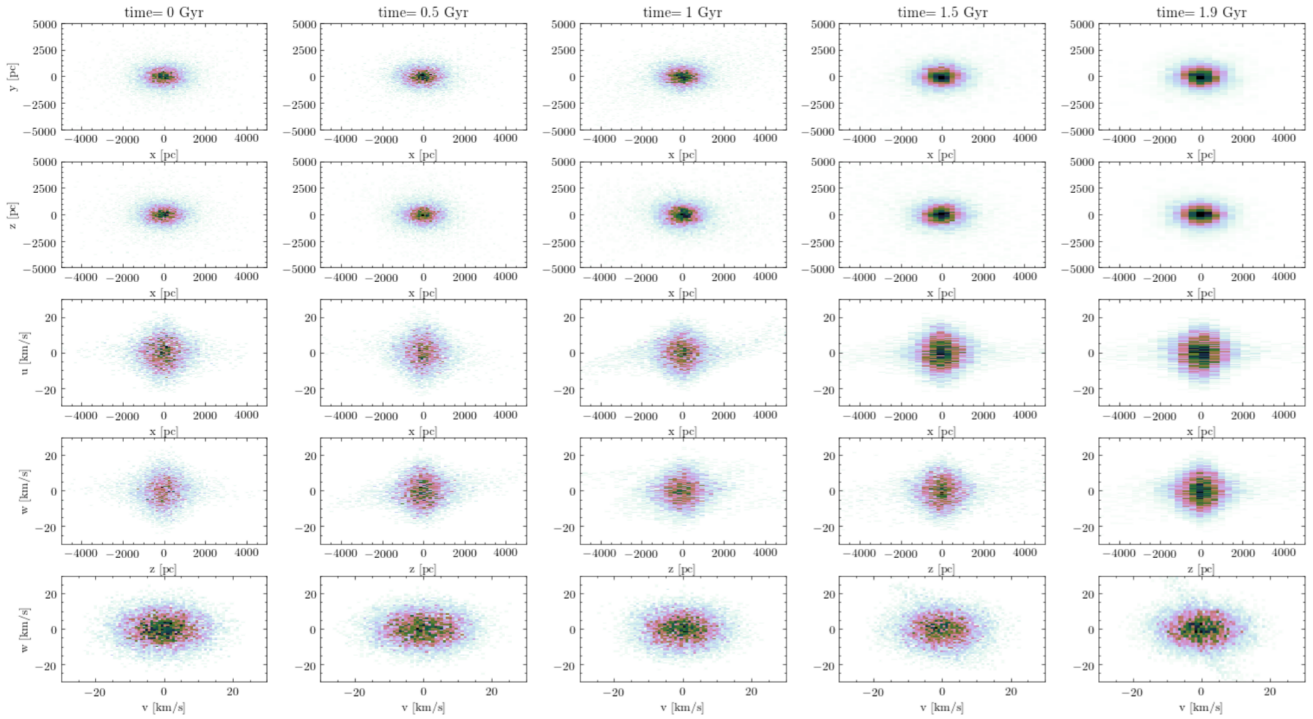

Figure 21: Core model 2D histograms in spatial (x, y, z) and velocity space (u, v, w) in the rest frame of the satellite, using the simpler formulation described in section 4.2 for a total mass of $10^8 M_\odot$.The pericentre passage happens at 600 Myr, so between the second and third column starting from the left.

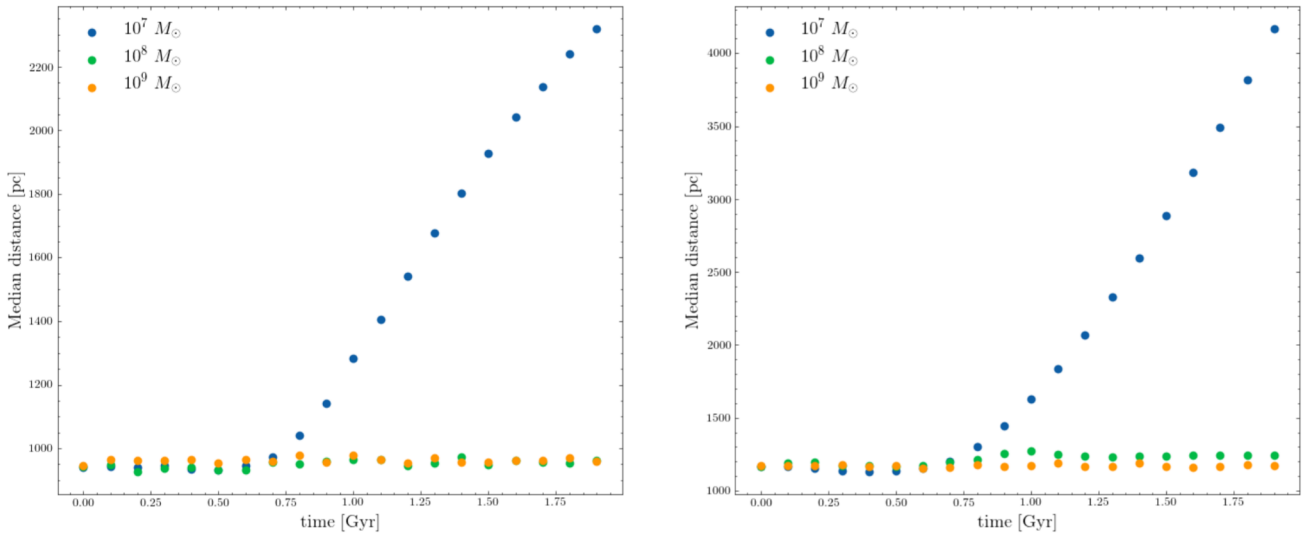

Figure 22: Median of space location at each time step of the simulation for each respective mass. **Left**: Cusp profile. **Right**: Core profile.

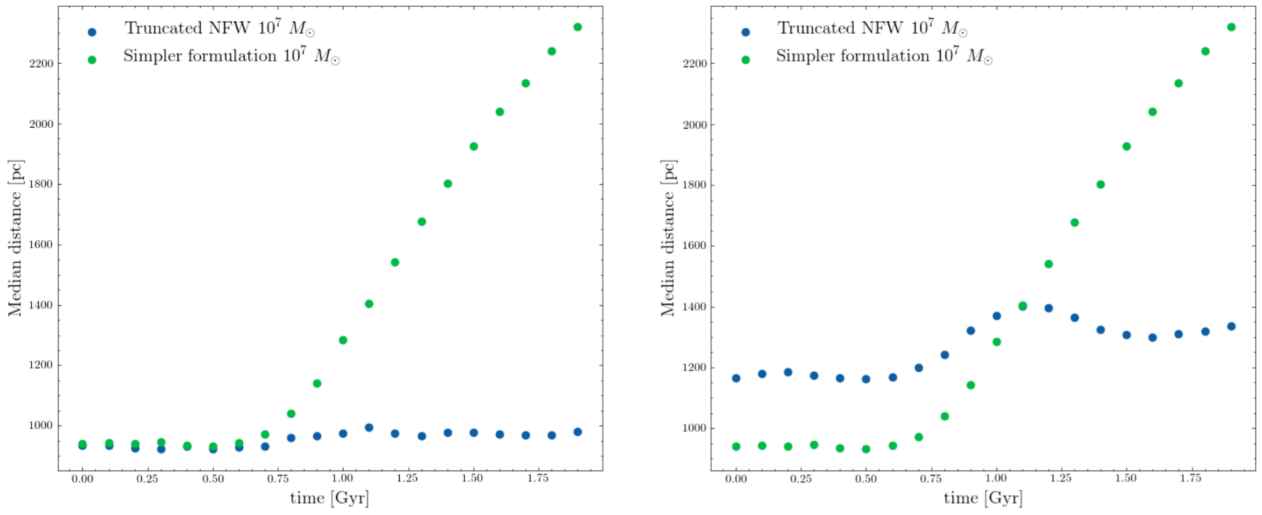

Figure 23: Median of space location of each system generated from eq.6 of chapter 3, truncated NFW, versus the median location obtained from the simpler formulation. **Left**: Cusp profile. **Right**: Core profile.

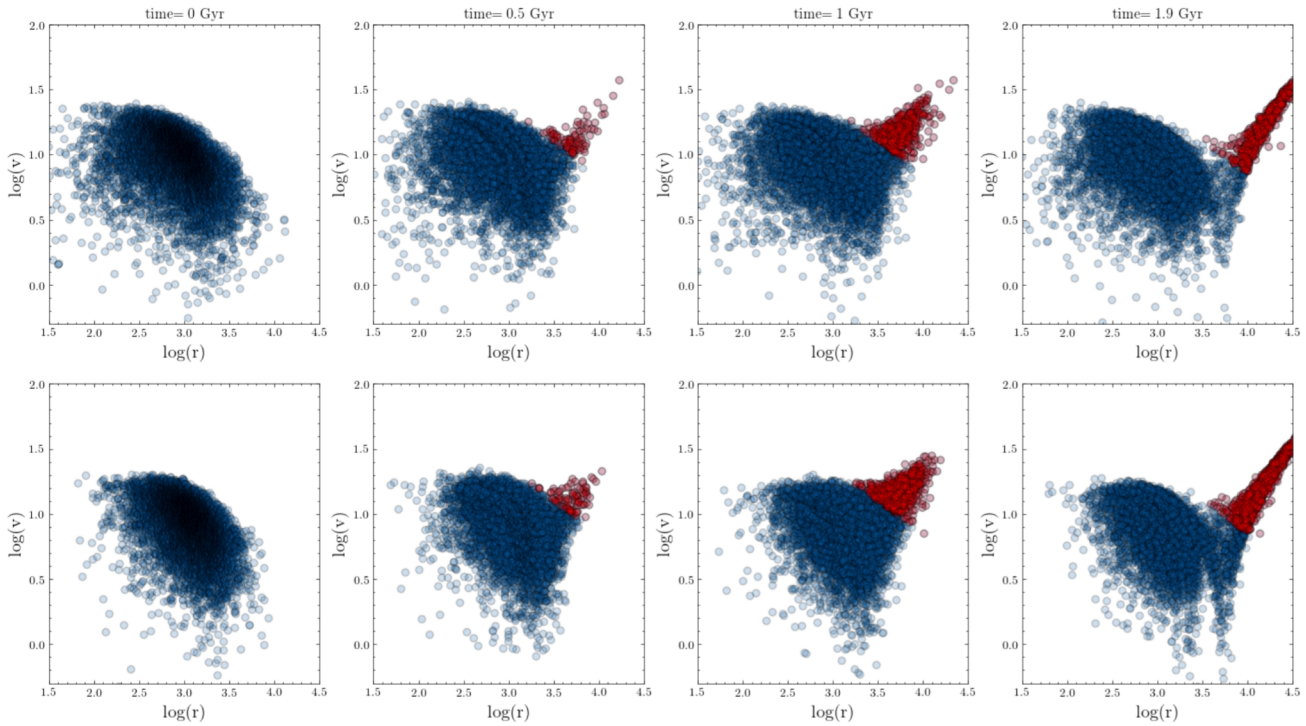

Figure 24: Rough estimation of particles that could become unbound from each of the models, when using a NFW truncated profile for a $M_{200} = 3 \cdot 10^8 M_\odot$. The particles were categorised as unbound when their kinetic energy would surpass the potential one, making their total energy greater than zero. This would need to be refined, since the mass is overestimated towards the end of the simulation, as the calculations were done considering the initial mass of the system. The number of particles that become 'unbound' for each model at each time stem would be for the Cusp model: [0, 88, 395, 560], while for the Core model:[0, 89, 654, 1045], out of 10^4 particles used in the simulation

Let there always be light (Searching for Dark Matter)

For this we go out dark nights, searching

For the dimmest stars,

For signs of unseen things:

To weigh us down.

To stop the universe

From rushing on and on

Into its own beyond

Till it exhausts itself and lies down cold,

Its last star going out.

Whatever they turn out to be,

Let there be swarms of them,

Enough for immortality,

Always a star where we can warm ourselves.

Let there be enough to bring it back

From its own edges,

To bring us all so close we ignite

The bright spark of resurrection.

Rebecca Elson